

Optical Spectroscopy of the Surface Population of the ρ Ophiuchi Molecular Cloud: The First Wave of Star Formation

Bruce A. Wilking

*Department of Physics and Astronomy, University of Missouri-St. Louis
1 University Boulevard, St. Louis, MO 63121
bwilking@umsl.edu*

Michael R. Meyer

*Steward Observatory, The University of Arizona, Tucson, AZ 85721
mmeyer@gould.as.arizona.edu*

John G. Robinson

*Department of Physics and Astronomy, University of Missouri-St. Louis
1 University Boulevard, St. Louis, MO 63121
johnr@newton.umsl.edu*

and

Thomas P. Greene

*NASA/Ames Research Center, M.S. 245-6
Moffett Field, CA 94035-1000
tgreene@mail.arc.nasa.gov*

ABSTRACT

We present the results of optical spectroscopy of 139 stars obtained with the Hydra multi-object spectrograph. The objects extend over a 1.3 square degree area surrounding the main cloud of the ρ Oph complex. The objects were selected from narrowband images to have H α in emission. Using the presence of strong H α emission, lithium absorption, location in the Hertzsprung-Russell diagram, or previously reported x-ray emission, we were able to identify 88 objects as young stars associated with the cloud. Strong H α emission was confirmed in 39 objects with line widths consistent with their origin in magnetospheric accretion columns. Two of the strongest emission-line objects are young, x-ray emitting brown dwarf candidates with M8 spectral types. Comparisons of the bolometric luminosities and effective temperatures with theoretical models suggest a median age for this

population of 2.1 Myr which is significantly older than the ages derived for objects in the cloud core. It appears that these stars formed contemporaneously with low mass stars in the Upper Scorpius subgroup, likely triggered by massive stars in the Upper-Centaurus subgroup.

Subject headings: stars: formation – stars: pre-main-sequence – ISM: individual (ρ Ophiuchi cloud) – open clusters and associations: individual (Upper Scorpius)

1. Introduction

Nearby molecular clouds which are the sites of active star formation are observed to be surrounded by a population of less obscured and more evolved young stars. $H\alpha$ emission-line and x-ray surveys have revealed large numbers of pre-main sequence stars that extend well beyond the molecular cloud boundaries. For example, the ROSAT All-Sky Survey has led to the identification of 112 lithium-rich pre-main sequence stars that are spread over a 450 square degree area surrounding the Orion star-forming molecular clouds (Alcalá *et al.* 1996). While some of the young stars appear to be related to earlier star formation in Gould’s Belt, at least 60% are found directly associated with the Orion molecular cloud complex (Alcalá *et al.* 2000). Proposed origins for these associated young stars include formation in rapidly moving cloudlets that have since dispersed (Feigelson 1996) or ejection from the cloud core due to three-body encounters (Sterzik & Durisen 1995). Alternatively, they could simply be fossil tracers of previously existing dense molecular gas in analogy with OB associations and now dispersed giant molecular clouds (e.g., Blaauw 1991). Clearly, determining the age and distribution of pre-main sequence stars surrounding the denser molecular gas holds the key to describing the star formation history of a region and perhaps sets limits to the lifetime of the molecular cloud.

The ρ Oph cloud complex, located the the edge of the Upper Scorpius subgroup in the Sco-Cen OB association, is comprised of a series of filamentary dark clouds that extend eastward from cores of dense molecular gas (de Geus 1992). At a distance of about 150 pc, it is one of the closest regions of active star formation. The main cloud, L1688, hosts a 1 pc x 2 pc centrally condensed molecular core where the visual extinction is estimated to be 50-100 mag (Wilking & Lada 1983). The core of L1688 has been the focus of numerous near-infrared, far-infrared, and millimeter continuum surveys, as well as x-ray and radio continuum surveys, and is found to host an embedded infrared cluster with around 200 stars (e.g., Greene & Young 1992; Bontemps *et al.* 2001; André & Montemerle 1994; Gagné, Skinner, & Daniel 2004). Infrared spectroscopic studies infer a median age of 0.3 Myr for objects in the core (Greene & Meyer 1995; Luhman & Rieke 1999). It has been suggested

that star formation in the ρ Oph core is the latest in a chain of events that began with massive stars in the Upper Centaurus-Lupus and Lower Centaurus-Crux subgroups of the Sco-Cen OB association triggering the formation of OB stars in the Upper Scorpius subgroup, which in turn initiated star formation in the L1688 cloud (de Geus 1992).

Until recently, there has been limited study of the nature of lightly extincted association members at the periphery of the L1688 cloud that have been identified through $H\alpha$ objective prism and x-ray surveys (e.g., Dolidze & Arakelyan 1959; Wilking, Schwartz, & Blackwell 1987; Montmerle *et al.* 1983; Casanova *et al.* 1995). Early spectroscopic studies of $H\alpha$ emission-line stars presented spectral types for about 20 young stars (Struve & Rubkjöbing 1949; Cohen & Kuhl 1979; Rydgren 1980). An optical spectroscopic survey of ρ Oph x-ray sources was conducted by Bouvier & Appenzeller (1992) and established spectral types for 30 pre-main sequence stars (23 new). They found an age of 1-10 Myr for these objects, significantly older than the age of objects in the core (see also Greene & Meyer 1995). But these samples favored the brighter association members and gave the incorrect impression that there was a deficiency of M spectral-type stars relative to other nearby star-forming regions (see Fig. 24, Hillenbrand 1997). This was remedied in part by Martín *et al.* (1998) who obtained optical spectroscopy for 59 ROSAT-selected sources in the core and streamer of the cloud with the majority of objects classified as pre-main sequence M stars. By examining the ratio of classical T Tauri stars (CTTS) to weak-emission T Tauri stars (WTTS), they found evidence for an older pre-main sequence population outside of the L1688 core.

In an effort to identify more widely-distributed and/or older late-type association members, we have obtained deep narrowband images of a one square degree area encompassing the L1688 cloud and centered at the wavelengths of $H\alpha$ and [S II]. Shorter exposures at R and I were also obtained. This resulted in a sample of 282 candidate CTTS with $R < 20$ mag that had possible $H\alpha$ emission. This sample includes association members with greater obscuration and/or lower mass than targeted by previous surveys. Using the multi-object spectrograph Hydra, optical spectra were obtained for 129 candidate CTTS plus 10 additional objects with $R < 19.1$ mag. Our sample selection procedure and the observations are described in Sec. 2. In Sec. 3, we detail our criteria for spectral classification and our examination of surface gravities. The results of the spectral classifications and an analysis of the emission-line spectra is given in Sec. 4. Also in Sec. 4, we list the criteria used to identify 88 association members from the sample and their locations in a Hertzsprung-Russell diagram. In Sec. 5, we compare the properties of the association members with those of low mass stars in the Upper Scorpius subgroup of the Sco-Cen OB association to gain insight into the star formation history of the ρ Oph cloud.

2. Observations and Data Reduction

Moderate resolution spectra were obtained for 129 of 282 stars identified as candidate CTTS from narrowband $H\alpha$ images of the ρ Ophiuchi cloud or from $H\alpha$ objective prism plates (Wilking *et al.* 1987). In addition, spectra were obtained for 5 bright association members and 5 brown dwarf candidates in the cloud not identified as candidate CTTS. A total of 139 stars were observed. These observations are described in detail in the sections below.

2.1. Sample Selection

The majority of candidate CTTS were selected from deep optical images of a one square degree area centered on the L1688 cloud obtained with the Curtis Schmidt Telescope at Cerro Tololo Interamerican Observatory. The images were obtained on 1995 March 10 and their reduction are described elsewhere (Wilking *et al.* 1997). Briefly, long (45 minute) exposure narrowband images centered at the wavelengths of $H\alpha$ (FWHM=64 Å) and [S II] (FWHM=45 Å) were obtained in addition to short (5 minute) exposures in the standard R and I bands. The latter were calibrated in the Johnson-Kron-Cousins photometric system using standard star fields established by Landolt (1992). R and/or I band photometry were obtained for over 2700 stars in the Ophiuchus field with $R < 20$. Accurate positions ($< 0.5''$) for these stars were obtained using the ASTROM program distributed by the Starlink Project and a set of secondary astrometric standards. The secondary position references were 27 $H\alpha$ emission line stars with accurate positions determined relative to SAO stars in a 5 square degree region on the Red Palomar Sky Survey plate (Wilking *et al.* 1987). The narrowband images were utilized to estimate the equivalent width of possible $H\alpha$ emission. The continuum in the $H\alpha$ filter was estimated using the flux in the [S II] filter after correcting for the differences in filter widths and transmission and assuming a flat continuum with no [S II] emission. The latter assumption was shown to be valid, with detections of weak [S II] emission in only two sources. As a result, 282 stars with $R < 20$ were identified with possible $H\alpha$ emission [$EW(H\alpha) > 10 \text{ \AA}$]. However, because of structure in the continuum due to reddening and photospheric absorption bands, it was desirable to confirm this emission spectroscopically.

2.2. Hydra Observations

One hundred fifty-one spectra were obtained for 139 stars located toward the cloud and its periphery on 1999 May 5-6 using Hydra, the multi-fiber spectrograph, on the WIYN 3.5m telescope¹. The Bench Spectrograph Camera was used with the red fiber cable, the 600 lines/mm grating with a blaze angle of 13.9° and the GG-495 filter to cover the range of 5820-8700 Å centered near 7200 Å. The spectral dispersion was 1.39 Å per pixel giving an effective resolution of 2.88 Å. The resolution at the central wavelength was $\lambda/\Delta\lambda=2500$. The program objects were selected by R magnitude, the H α equivalent width estimated from the narrowband images, and their accessibility to a fiber. Program objects were distributed among four fiber configurations sorted by R magnitude; twelve program stars were observed in two configurations. Field 1 included the brightest candidate CTTS (R<15) and, to make most efficient use of the spectrograph, 5 bright x-ray sources known to be association members but with no known H α emission. Fields 2 and 3 sampled the same magnitude range of candidate CTTS (15<R<17) with the pointing centers shifted in declination. Field 4 candidates (17<R<19.1) were supplemented by 5 brown dwarf candidates from the study of Wilking, Greene, & Meyer (1999). We observed 81% of the candidate CTTS with R<15, 88% of the candidates with 15<R<17, 45% with 17<R<18, and 21% of the candidates with 17<R<19.1. In Table 1, we summarize the observations by presenting for each field the pointing center, R magnitude range, number of candidate CTTS observed, integration time, and number of exposures.

The spectra were reduced using the Image Reduction and Analysis Facility (IRAF).² Images were processed for bias and dark corrections using CCDPROC. Multiple exposures of a given field were median-combined and then reduced with IRAF’s DOHYDRA package. The images were flat-fielded using dome flats obtained for each fiber configuration except for Field 1 where the flat from the configuration for Field 2 was used. Sky subtraction was accomplished using the median of 7-10 sky spectra distributed across each field. The spectra were wavelength calibrated using 5 second exposures of CuAr lamps. Scattered light corrections were not made and no flux calibration was performed. It was necessary in a few cases to improve the sky subtraction by first scaling the median sky spectrum before subtracting it from the source spectrum. The typical signal-to-noise for the spectra extracted in each field is presented in Table 1.

¹The WIYN Observatory is a joint facility of the University of Wisconsin-Madison, Indiana University, Yale University, and the National Optical Astronomy Observatory.

²IRAF is distributed by NOAO for AURA, Inc.

3. Analysis of the Spectra

Spectral types were derived from visual classification (visual pattern matching of our smoothed program star spectra with standard star spectra) supported by quantitative analysis of some spectral indices. In this section, we provide descriptions of the absorption lines used to classify three broad groups, starting with the earliest spectral type stars (B-A), moving to the F-K stars, and finally the M stars. We conclude the section with a discussion of gravity-sensitive absorption features in the 5820-8700 Å spectral range. For the purposes of matching spectral features with those of standard stars, our Hydra spectra were smoothed using a gaussian filter to the resolution of the standard stars for direct comparison. All spectra have been normalized to 1 by dividing out a fit to the continuae, carefully excluding regions with emission lines or broad absorption due to TiO and VO. Normalized spectra smoothed to a resolution of 5.7 Å are shown in Fig. 1 for a representative sample of program objects, with early-type stars in Fig. 1a (B3-G9), K stars in Fig. 1b, early-to-mid M stars in Fig. 1c, and mid-to-late M stars in Fig. 1d. Both photospheric and telluric spectral features are labeled.

Two main sets of standards were used for classification (both qualitative and quantitative). First, optical spectra from the WIYN/Hydra study of the Praesepe by Allen & Strom (1995) were used to derive spectral types from B8V - M4V. The effective resolution of these spectra was 5.7 Å. For giants and later type dwarfs (M5V - M9V), optical spectra from the study of Kirkpatrick, Henry, & McCarthy (1991) were used with an effective resolution of either 8 or 18 Å. In addition to these, optical spectra of very late type subgiants in IC 348 (Luhman 1999) and ρ Oph (Luhman, Liebert, & Rieke 1997) were used for comparison with the coolest stars in our sample. For stars earlier than B8V, we referred to the spectral atlas of Torres-Dodgen and Weaver (1993).

3.1. Classification of B-A Stars

Absorption lines from the Balmer ($n=2$) and Paschen ($n=3$) series of hydrogen are prominent in the spectra of early type stars. In our spectra, we see unblended absorption lines from $H\alpha$ (6563 Å) and Paschen 14 (8598 Å) (see Fig. 1a) that reach a maximum around A0 and weaken in warmer stars. The Ca II triplet (8498 Å, 8542 Å, 8662 Å) is also observed and decreases in strength toward early-type stars until overtaken by Pa 16, 15, and 13 (8502Å, 8545Å, and 8665Å). Hence an F2 star may have a similar $EW(H\alpha)$ as a B5 star, but will be distinct by displaying stronger absorption from the Ca II triplet. We note that all of the aforementioned lines can appear in emission, and that the observed absorption line strengths could be lower limits to the true strengths. We estimate that the uncertainties

in our derived spectral types in this range is ± 5 subclasses, however, our adopted spectral types will be greatly aided by previously published observations of these intrinsically bright stars.

3.2. Classification of F-K5 Stars

The relative strength of absorption due to $H\alpha$ and a blend of Ba II, Fe I, and Ca I centered at 6497 Å is the most sensitive indicator of spectral type over this range. Also helpful in spectral classification is absorption due to Ca I at 6122 Å which grows stronger from A to K spectral types (e.g., compare Figs. 1a and 1b). Absorption from the Ca II triplet is present but shows little variation with spectral type in F-K stars. In general, the variation in these features is very gradual from subclass to subclass and, when coupled with the signal-to-noise of the spectra, the uncertainties in the spectral classifications between F0 and K0 are often ± 3 -5 subclasses. Paschen line absorption (13 and higher transitions) will be present through mid-F stars, but Pa 13, 15, and 16 are blended and dominated by the lines from the Ca II triplet at our resolution. Once again, the partial filling of $H\alpha$ absorption by $H\alpha$ emission in CTTS could lead us to assign spectral types that are too late.

3.3. Classification of K5-M9 Stars

For stars K5V and later, the depths of the TiO and VO bands provide the most sensitive indicators of spectral type. As shown in Fig. 1b, TiO absorption bands begin to appear in mid-K stars centered at 6300 Å, 6700 Å, and 7140 Å and increase in strength through M6V stars (Fig. 1c). Absorption due to TiO, which begins near the strong telluric O₂ band (“oxygen B band”, 7594-7685 Å) and extends to 7861 Å, is evident for spectral types of M1V and later and is further strengthened by VO absorption from 7851-7973 Å in mid-to-late M stars (Fig. 1d). TiO absorption bands from 8432-8452 Å also appear for spectral types of M2V and later and increase in strength through M9V (Fig. 1d). For the coolest M stars (M6-M9), the depths of the TiO bands centered at 7140 Å and 7800 Å appear to decrease, likely due to depletion of Ti into grains (e.g., Allen 1996, Fig. 2a); VO absorption from 7334-7543 Å and from 7851-7973 Å then becomes a more reliable indicator of spectral type.

Spectral classification in this temperature range was accomplished through a combination of visual classification and quantitative analysis of TiO and VO indices which we now describe. The indices were computed by taking the ratio of the average flux in a ~ 50 Å wide band of the continuum to the average in an absorption band. Following Allen (1996),

we plotted the TiO index of $7035\text{\AA}/7140\text{\AA}$ vs. the TiO index of $7500\text{\AA}/7800\text{\AA}$ along with their one sigma errors for each Hydra field as well as our dwarf standards. Fig. 2a shows a plot of the TiO indices for the dwarf standards. There is a general trend for TiO index to increase with later spectral type until M7, where the trend reverses and the index decreases for stars cooler than M7. To resolve the ambiguity caused by this reversal, we developed two narrow band VO indices for spectral classification of the coolest stars in our sample. A plot of these indices is shown in Fig. 2b for M dwarf standards. The first index is the ratio of the continuum averaged over two bands which bracket the VO band centered at 7485\AA to the average flux in the VO band. The second index is the ratio of the continuum in a band centered on 8120\AA to the flux in the VO band centered at 7979\AA . As shown in Fig. 2b, there is a general trend for the indices to increase from spectral types M3 to M9. While the use of these indices allowed us to sort objects by temperature, the final spectral classifications were made by direct comparisons of the strengths of the TiO and VO bands with standard star spectra. The sensitivity of these absorption bands to spectral class allowed us in most cases to estimate M spectral types to within a subclass.

3.4. Surface Gravities

A rough estimate of the surface gravity of an object is important in determining its nature and in estimating accurately its effective temperature for a given spectral type. In particular, surface gravity indicators can help identify background giants and field dwarfs that might contaminate our sample. Gravity-sensitive absorption features available for analysis in our spectra include the CaH band centered at 6975\AA and the Na I doublet at $8183/8195\text{\AA}$ (both strongest in dwarfs) and absorption from the Ca II triplet at 8660\AA (strongest in giants). Of these features, CaH is well-positioned for study.

Following Allen (1996), we have calculated a CaH index as the ratio of the continuum at $7035\pm 15\text{\AA}$ to the flux in the CaH absorption band at $6975\pm 15\text{\AA}$ and a TiO index as the ratio of the continuum at $7030\pm 15\text{\AA}$ to the flux in the TiO absorption band at $7140\pm 15\text{\AA}$ from the normalized spectrum of each program object. In Fig. 3, we plot the CaH index vs. the TiO index for 136 program objects. Error bars are computed based on the one-sigma error in flux averages and propagated to the ratios. The solid lines represent first or second order fits to the standard star spectra. Based on this plot, we conclude that the surface gravities for objects with the largest TiO index (coolest stars) are intermediate between those of giants and dwarfs. While there are clearly late-type giants present in our sample, about 70% of the program objects have TiO indices < 2 (about spectral type M4 V) and surface gravities that most closely resemble dwarf stars. Therefore, spectral types for our

program objects were determined by comparing them to a grid of dwarf standards.

4. Results

Spectral types were determined for 131 of 139 stars in the manner described in Sec. 3.3. Using the CaH index and other gravity sensitive features (Sec. 3.4), six stars are identified as giants and 26 as possible dwarfs. These data are presented in Table 2 along with any previous source names, x-ray associations, RA and DEC in J2000, and R and I magnitudes. The derived spectral types (or range of possible spectral types) are also shown to the right of each spectrum in Fig. 1 along with its classification as a possible dwarf (V?), giant (III), association member (A), or association unknown (U). The top two spectra in Figs. 1c and 1d demonstrate the different features present in high and low surface gravity objects of the same spectral type. In the following sections, we discuss what the spectra reveal about the characteristics of the young stars and their evolutionary states. Included in this discussion is the distribution of spectral types in our sample and the variety and properties of their emission lines. A description is given of how association membership was determined and the resulting spatial distribution of association members relative to the molecular gas. Finally, the evolutionary state of the population is estimated by deriving ages and masses using a Hertzsprung-Russell diagram.

4.1. Distribution of Spectral Types

The distribution of spectral types for our sample is shown in Fig. 4. Over half (79) of the 131 objects with spectral-type determinations are M stars. The fact that our sample is dominated by M stars is due in part to a selection effect caused by the onset of TiO absorption bands. The procedure described in Sec. 2.1 was designed to select objects with H α emission provided the continuum was relatively flat. But the same procedure could erroneously identify M stars with strong TiO absorption as H α emission-line objects since the H α filter bandpass lies in a spectral region free of TiO absorption while the comparison [S II] filter bandpass lies within strong TiO absorption at 6700 Å.

The shaded areas of the histogram represent sources with strong H α emission ($EW(H\alpha) > 10 \text{ \AA}$) at the time of our observations. Our procedure of selecting H α emission line stars from narrowband images was only moderately successful. In particular, our procedure appears to break down for the fainter sources ($R < 17$) which accounts for the number of background G stars in our spectroscopic sample. Our highest success rate occurred with mid-K stars and

mid-to-late M stars and was 65%. In the latter group, H α emission was clearly a factor in their identification in our original narrowband image. There is clearly no deficiency of M-type CTTS in the ρ Oph cloud relative to other nearby star-forming regions. The apparent lack of M stars in previous spectroscopic surveys represents the bias toward brighter stars in those surveys.

4.2. Emission-Line Spectra

Nearly one-third of our sample for which we could determine spectral types displayed strong emission from H α . The spectra for about one-third of these strong emitters also exhibited emission lines from He I, O I, Ca II, and/or Pa 14. Emission lines were identified and their equivalent widths and full-widths at half maximum (FWHM) were measured using gaussian fits. No attempt was made to deconvolve the emission profile by the instrument response. The results for all CTTS are presented in Table 3.

Since our sample was based on a procedure designed to select sources with strong H α emission characteristic of CTTS, it is not surprising that 39 of the 131 objects with spectral-type determinations displayed strong H α emission. Of these, 26 are newly identified CTTS based on an $\text{EW}(\text{H}\alpha) > 10 \text{ \AA}$ criteria. The previously identified CTTS can be found in Table 2 by looking at sources with previously measured H α emission (column 10). An additional 17 objects showed weaker H α emission ($10 \text{ \AA} > \text{EW}(\text{H}\alpha) > 5 \text{ \AA}$) with nearly all having spectral types from M3-M5. We note that variability plays a role in the identification of H α emission (e.g., Wilking *et al.* 1987; Hartigan 1993). Among the six H α emitters with multiple observations, the equivalent width of Object 2-30 (field number-aperture from Table 2) dropped from 38 \AA to 8.5 \AA in only one day. The brown dwarf candidate GY 5 was observed to have an $\text{EW}(\text{H}\alpha) = 15 \text{ \AA}$ whereas a similar spectrum obtained in 1998 showed no detectable emission (Wilking *et al.* 1999). In addition, the shape of the emission profile also appeared to change in three cases (Chini 8, EL 24, and Object 2-30). All of the strong H α emission lines were well-resolved with typical FWHMs of 250 km s^{-1} compared to the 128 km s^{-1} velocity resolution of our data.

These broad H α profiles, which can exceed 300 km s^{-1} in our sample, have been successfully modeled as arising in magnetospheric accretion columns (Hartmann, Hewett, & Calvet 1994; Muzerolle, Calvet, & Hartmann 2001). Thirteen of the H α profiles were clearly asymmetric or displayed non-gaussian wings. The profile shapes are noted in Table 3 using the classification scheme of Reipurth, Pedrosa, & Lago (1996). The prevalence of wings or asymmetries on the blue-side of the profile is typical among CTTS and suggests the presence of mass outflows. The Ca II triplet at 8660 \AA was observed in emission in 14 of the H α

emitters and was strongest in the G or K spectral type objects. No attempt was made to deblend them from the weaker Paschen emission lines Pa 13, Pa 15, and Pa 16. In general, the Ca II lines were narrower than H α and barely resolved in our data with typical FWHMs of 150 km s⁻¹. Fig. 5 shows an expanded view of the H α emission and Ca II emission lines for a representative sample of 7 CTTS. As in Fig. 1, the spectra have been smoothed to a resolution of 5.7 Å. H α profiles for objects 1-24 and 1-29 were symmetric while the rest of the profiles in Fig. 5a exhibited a blueward asymmetry. Only the source Object 2-31/1-35 (bottom two spectra in Fig. 5a and 5b) displayed asymmetric profiles in both Ca II and H α .

Emission lines from both permitted and forbidden atomic transitions were detected in the spectra of the strongest H α emitters in Table 3 with EW(H α) > 28 Å. Both Pa 14 and O I (7773 Å) displayed broad profiles with FWHMs similar to that of H α . The other O I lines and the He I lines all appeared to be barely resolved, with FWHMs between 150-180 km s⁻¹. The detection of forbidden line emission from [O I] was observed in 6 objects. Weak [S II] emission at 6731 Å was detected in only 2 objects (SR 22 and WSB 46). The detection of these lines is consistent with the presence of winds associated with CTTS (Edwards *et al.* 1987).

4.3. Identification of Pre-Main Sequence Association Members

Pre-main sequence objects (PMS) objects that are products of recent star formation in the Ophiuchus region were identified using one or more of the following four criteria. First, candidates with H α emission with EW > 10 Å resemble CTTS, a property exhibited by 39 stars in our study (see col. 11, Table 2). Second, association with x-ray emission is a signpost of youth and has been observed in 52 stars from our sample by various surveys of the region (see col. 4, Table 2). Third, the presence of lithium absorption is an indicator of youth. While the lithium absorption was not well-resolved in our spectra, it was definitely detected in 30 stars (col. 9, Table 2). Finally, 58 objects (excluding giants identified in Sec. 3.3) that are too luminous to be main sequence objects at the distance to ρ Oph *and* have an estimate for A_v too high to be foreground to the cloud ($A_v > 1.5$ mag) are identified as pre-main sequence objects. Table 4 lists the 88 association members identified by our observations followed by the criteria used in their classification. At least 25 of these objects are newly identified association members. The bright association member SR 12 has been included in list; while we did not obtain a spectrum, it was present in our R and I band images and had a previously well-determined spectral type.

We note that of the 26 objects with dwarf-like surface gravities (Table 2), 19 are identified as association members based on criteria 2, 3, or 4. None display strong H α emission.

Without performing a quantitative analysis, the strengths of their CaH and Na I absorption lines are indistinguishable from main sequence stars.

4.3.1. Lithium

The presence of Li I absorption at 6707 Å in stellar spectra indicates the objects have cool interiors ($<2 \times 10^6$ K) and are young. Measurements proved to be difficult for most objects due to our spectral resolution and neighboring iron lines. The line was definitely observed in 30 stars with higher S/N spectra (“yes” in col. 9, Table 2) and tentatively detected in 19 stars (“yes:” in col. 9, Table 2). Six stars were identified as young objects solely on the basis of lithium absorption (Table 4) and all were located above the main sequence in the H-R diagram. The absence of an Li entry in Table 2 or Table 4 does not imply that Li I is not present, only that the feature was not discernable in our spectra.

4.3.2. Brown Dwarfs

This program included 7 brown dwarf candidates identified through low resolution infrared spectroscopy: GY 3, GY 5, GY 37, GY 59, GY 204, GY 310, and GY 326 (Wiling, Greene, & Meyer 1999, hereafter WGM99; Luhman & Rieke 1999; Natta *et al.* 2002). The new optical spectral types agreed with the infrared classifications within 2 subclasses for 6 out of 7 sources. Using infrared spectra, GY 310 was classified as an M8.5 by WGM99 and Wiling, Meyer, & Greene (2005), and M6 by Natta *et al.* (2002). While the spectrum is noisy, our optical classification of M4 for GY 310 is significantly earlier and, if confirmed, may suggest the presence of an infrared companion.

The two coolest objects in our sample, 4-41 (GY 3) and 4-45 (GY 264), are classified with M8 spectral types. Their spectra, shown in Fig. 1d, feature strong VO absorption at 7334-7534 Å and 7851-7973 Å. The shorter wavelength VO forms a obvious depression in the continuum between two TiO bands. The longer wavelength VO broadens the absorption from the 7666-7861 TiO band starting around 7900 Å. Their classifications as young brown dwarf candidates was confirmed by their strong H α emission [EW(H α) = 140 Å and 155 Å, respectively], association with x-ray emission (see Table 2), and location in the H-R diagram (Sec. 4.4). Object 4-41, also known as ISO Oph 32, was first identified as a low mass object by Natta *et al.* (2002). Excess emission at K ($(r_k) = 0.34$) and in the mid-infrared

(Bontemps *et al.* 2001) are indicative of a circumstellar disk (Natta *et al.* 2002)³. Object 4-45 is a previously unidentified brown dwarf candidate. It was previously misidentified as a foreground M star based on VRI photometry (ophmd5, Festin 1998). It does not appear to have an infrared excess with $r_k = 0.02$. The object lies in close proximity to the “marginal” Herbig-Haro candidate P2 (Phelps & Barsony 2004).

4.3.3. Distribution of Association Members

The distribution of the 88 association members identified by this study is shown in Fig. 6 relative to contours of ^{13}CO column density which delineate the cloud boundaries. We note that due to the high extinction in the cloud core, our data samples only the surface population toward the densest gas. For reference, star symbols mark the locations of the Sco-Cen B star ρ Oph A and the the most massive member of the L1688 embedded cluster, Oph S1. There is a definite tendency for association members to concentrate near the highest column density gas in the core. Only 14 members are seen in projection outside the lowest contour corresponding to $N_{LTE}(13) = 6 \times 10^{14} \text{ cm}^{-2}$.

4.4. Hertzsprung-Russell Diagram

With the benefit of the spectroscopic data, we can investigate the ages and masses of the association members identified by this study. The intrinsic colors, bolometric corrections, and temperature scale for dwarf stars were derived from the works of Schmidt-Kaler (1982) for B8-K5 stars and from Bessell (1991) for K5-M7 stars. We note that the assumption of dwarf, rather than subgiant, surface gravities will overestimate T_{eff} for stars with spectral types of G5-K5 by <250 K and underestimate T_{eff} for stars with spectral types of M2-M8 by <200 K. For the B3 star Source 1, an effective temperature of $T_{eff} = 19,000$ and an $L_* = 1500 L_\odot$ was adopted (e.g., Lada & Wilking 1984). For the M8 brown dwarf candidates, we assumed values of $T_{eff} = 2500$, $(R - I)_0 = 2.5$, and $BC(I) = -1.7$ that are consistent with recent studies of very low mass stars (Dahn *et al.* 2002; Hawley *et al.* 2002). Bolometric luminosities were computed from the I band magnitudes in the following way. Magnitudes were dereddened using the (R-I) color excess derived from the observed

³Using JHK photometry from the 2MASS catalog converted into the CIT photometric system, $r_k = F_{Kex}/F_K = [(1+r_h)(10^{[(H-K)-(H-K)_0-0.065*A_v]/2.5})]-1$ where $r_h = F_{Hex}/F_H = (10^{[(J-H)-(J-H)_0-0.11*A_v]/2.5})-1$ with intrinsic colors and visual extinctions computed for an M8 spectral type.

minus intrinsic (R-I) color for the corresponding spectral type and using the reddening law $A_v/E(R-I) = 6.25$ (Cohen *et al.* 1981). In a few cases the errors in the photometry and/or spectral classification yielded slightly negative values for the extinction and an extinction of 0.0 was assumed. Absolute I magnitudes were then computed assuming a distance of 150 pc (de Zeeuw *et al.* 1999) and converted to bolometric magnitudes using the appropriate bolometric correction for the observed spectral type. The stellar luminosity was computed using $\text{Log}(L/L_\odot) = 1.89 - 0.4 \times M_{bol}$ assuming $M_{bol\odot} = 4.74$ (Livingston 1999). Due to the dominance of emission lines in the spectrum of WL 18, we adopted the luminosity estimated by Bontemps *et al.* (2001) from the J band flux and (J-H) color, adjusted to a distance of 150 pc.

The resulting H-R diagram is presented in Fig. 7 for 84 association members relative to the theoretical tracks and isochrones of D’Antona & Mazzitelli (1997, 1998). Excluded from the diagram is the B3 star Source 1, the A7 star VSSG 14, and objects GY 59 and GY 326 which lack R band photometry and therefore estimates for A_v and $\text{Log}(L)$. CTTS are marked by the solid diamonds; open diamonds mark association members with weak or no $H\alpha$ emission that would correspond to weak-emission or post T Tauri stars. The errors in T_{eff} are estimated to be ± 105 K for K-M stars with equal contributions from the uncertainties in the spectral classification and systematic offsets in the temperature scale. The uncertainty in $\text{Log}(L)$ is estimated to be 0.12 dex, assuming uncertainties in the R and I photometry of 0.04 mag, in the distance modulus of 0.15 mag, and in the bolometric correction of 0.1 mag. The masses and ages interpolated from the models are given in Table 4 with uncertainties due to random errors of 20% in mass and 0.25 dex in $\text{Log}(\text{age})$. Comparisons with the Baraffe *et al.* (1998) models suggest systematic errors between different sets of models of $\sim 50\%$ in mass and ~ 0.5 dex in $\text{Log}(\text{age})$ (e.g., Hillenbrand & White 2004).

The median age of the association members in Fig. 7 is 2.1 Myr. There is no significant difference observed in the median age of the CTTS and the non-CTTS association members. Following the analysis of Preibisch & Zinnecker (1999), the apparent age spread observed in Fig. 7 is consistent with all of the association members having roughly the same age (1-3 Myr) with the scatter in the age accounted for by the errors noted above and unresolved binaries.

5. Implications for the Star Formation History

The association members identified in this study are pre-main sequence objects distributed over a 1.3 square degree area (6.8 pc^2) and lie within a projected radius of 2 pc of the highest extinction regions of the main ρ Oph cloud (see Fig. 6). The fact that our

derived visual extinctions are generally low (80% of the association members have $A_v \leq 5$ mag) indicates that the majority of our sample lies at the surface of the cloud. Recent spectroscopic studies of YSOs in the ρ Oph cloud have focussed on the embedded population in the 1 pc x 2 pc centrally condensed core and have necessarily been conducted at near-infrared wavelengths (Greene & Meyer 1995; Luhman & Rieke 1999; WGM99; Natta *et al.* 2002). These studies have consistently derived ages between 0.1-1 Myr when using the D’Antona & Mazzitelli tracks and isochrones, with a median age of 0.3 Myr. After considering our uncertainties, we conclude that the distributed population is significantly older than that in the more highly extincted cloud core.

The question then arises as to the origin of this more distributed population. One explanation is that these objects formed in the dense core and have diffused or been ejected to the surface of the cloud. However, the space motion of a YSO which acquires the velocity dispersion of the molecular gas in which it formed (1-2 km s⁻¹) would not be high enough to move an object to the projected distances from the core of >1 pc that we observe for some association members. Alternatively, the ejection of very low mass stars and brown dwarfs from small groups has been proposed for the origin of widely distributed WTTS and of substellar objects (Sterzik & Durisen 1995; Reipurth & Clarke 2001; Bate *et al.* 2002). In this case, one would predict that the lowest mass association members in our sample would display a higher velocity dispersion (and thus a broader spatial distribution) than YSOs in the core. We have analyzed the distribution of the higher mass association members ($M > 0.5 M_\odot$) relative to the lower mass members ($M < 0.5 M_\odot$) using a two-dimensional Kolmogorov-Smirnov (K-S) test. The K-S statistic is consistent with the two populations being drawn from the same parent population. Our data do not lend support to the ejection hypothesis, however our sample includes only 8 brown dwarf candidates.⁴

A second possibility is that the association members at the cloud edges are near their birthsites and that the dense gas in L1688 was once distributed over a larger area than we see today. It has been proposed that star formation in the Upper Scorpius was triggered about 5 Myr ago by the passage of an expanding HI shell driven by massive stars in the Upper Centaurus-Lupus association (de Geus 1992). This age is consistent with that of high mass stars in Upper Sco derived from a color-magnitude diagram and from the main sequence turnoff (Preibisch *et al.* 2002; see models by Bertelli *et al.* 1994). The implied age of the low mass stars in Upper Sco is also 5 Myr, but only after corrections are made for unresolved binaries (Preibisch & Zinnecker 1999). A comparison of Fig. 7 with H-R diagrams for low

⁴Radial velocity measurements are required for a detailed analysis of the kinematics of these stars to reject the hypothesis that they were ejected from the cloud as the result of the dissolution of small stellar groups.

mass members of the Upper Scorpius subgroup, using the same set of theoretical evolutionary tracks and isochrones and not corrected for unresolved binaries, shows no discernable difference in age or age spread (e.g., Preibisch & Zinnecker 1999; Preibisch, Guenther, & Zinnecker 2001; Preibisch *et al.* 2002). This is not too surprising given that the ρ Oph cloud is ringed by high-mass members of Upper Scorpius such as the multiple star ρ Oph and σ Sco to the west and 22 Sco, α Sco, and τ Sco to the east. Therefore, one could regard the distributed population we observe as either low mass members of the Upper Scorpius subgroup or as older members of the ρ Oph cloud whose formation was contemporaneous with stars in the Upper Scorpius subgroup. In either scenario, ultraviolet radiation and the passage of an expanding shell from massive stars in the Upper Scorpius subgroup within the last 2.5 Myr would have stripped away the outer skin of the ρ Oph cloud, revealing the present population and perhaps triggering a second episode of star formation in the centrally condensed core (de Geus 1992).

6. Summary

We have analysed optical spectra for 139 candidate CTTS that extend over a 1.3 square degree area in the direction of the main ρ Oph cloud. Of the 131 stars for which spectral types and surface gravities are estimated, 6 are identified as giants and 79 are classified as M stars. Association with the cloud is established for 88 objects by the presence of optical emission lines or lithium absorption in the spectra, by location in the H-R diagram, and/or by previously reported x-ray emission. Thirty-nine of the stars display strong H α emission ($EW > 10\text{\AA}$) characteristic of CTTS. These emission lines are broad ($FWHM \sim 250 \text{ km s}^{-1}$), consistent with their origin in magnetospheric accretion columns. In addition, asymmetries in the H α profiles and the presence of forbidden lines are observed in 16 objects as a signpost of mass outflows. A subset of the CTTS also display emission from the Ca II triplet which is strongest in the most massive CTTS and, in one instance, self-absorbed. Two of the strongest emission-line objects are young, x-ray emitting brown dwarf candidates with M8 spectral types.

Association members are distributed in the lower extinction regions surrounding the high extinction core. A H-R diagram suggests a median age of 2.1 Myr with an apparent age spread due mainly to uncertainties in the calculated luminosity and the presence of unresolved binaries. This age is significantly older than the median age of 0.3 Myr for objects in the high extinction core. There is no difference in median age between the CTTS and non-CTTS association members and there are no statistically significant correlations between the age or mass of an association member and its projected distance from the core

center. The age and distribution of this population is indistinguishable from low mass stars in the Upper Scorpius subgroup. We propose that these stars formed in what was once a larger ρ Oph cloud. In this instance, star formation in the outer regions of the ρ Oph cloud would have been triggered by the same event that initiated star formation in Upper Scorpius.

We thank Di Harmer for obtaining the Hydra data through the WIYN Queue Observing Program and for assistance with the data reduction. Lori Allen provided helpful insight into the spectral typing process and made available the bulk of the spectral standards used in this study in digital form. We gratefully acknowledge Eric Mamajek for helpful discussions. MRM acknowledges support for this work through a Cottrell Scholar’s Award from the Research Corporation. BW and JR acknowledge support from NSF AST-9820898 to the University of Missouri-St. Louis and from the Missouri Research Board.

REFERENCES

- Alcalá, J. M., Terranegra, L., Wichmann, R. *et al.* 1996, *Astronomy & Astrophysics Supplement*, 119, 7
- Alcalá, J. M., Covino, E., Torres, G., Sterzik, M. F., Pfeiffer, M. J., & Neuháuser, R. 2000, *A&A*, 353, 186
- Allen, L. E. 1996, Ph.D. Thesis, University of Massachusetts
- Allen, L. E. & Strom, K. M. 1995, *AJ*, 109, 1379
- André, P., Montmerle, T., & Feigelson, E. D. 1987, *AJ*, 93, 1182
- André, P. & Montmerle, T. 1994, *ApJ*, 420, 837
- Bate, M. R., Bonnell, I. A., & Bromm, V. 2002, *MNRAS*, 332, 65
- Bertelli, G., Bressan, A., Chiosi, C., Fagotto, F., & Nasi, E. 1994, *Astronomy & Astrophysics Supplement*, 106, 275
- Baraffe, I., Charbrier, G., Allard, F., & Hauschuldt, P. H. 1998, *A&A*, 337, 403
- Bessell, M. S. 1991, *AJ*, 101, 662
- Blaauw, A. 1991, in *The Physics of Star Formation and Early Stellar Evolution*, eds. C.J. Lada & N.D. Kylafis, Kluwer Academic Publishers, Dordrecht, The Netherlands, p. 125
- Bontemps, S., André, P., Kaas, A., Nordh, L., Olofsson, G., Hultgren, M., Abergel, A., Blommaert, J., Boulanger, F., Burgdorf, M., Cesarsky, C., Cesarsky, D., Copet, E., Davies, J., Falgarone, E., Lagache, G., Montmerle, T., Pérault, M., Persi, P., Prusti, T., Puget, J., & Sibille, F. 2001, *A&A*, 372, 173
- Bouvier, J. & Appenzeller, I. 1992, *Astronomy & Astrophysics Supplement*, 92, 481
- Casanova, S., Montmerle, T., Feigelson, E. D., & André, P. 1995, *ApJ*, 439, 752
- Chini, R. 1981, *A&A*, 99, 346
- Cohen, M. & Kuhl, L. V. 1979, *ApJS*, 41, 743
- Cohen, J. G., Frogel, J. A., Persson, S. E., & Elias, J. H. 1981, *ApJ*, 249, 481
- Dahn, C. *et al.* 2002, *AJ*, 124, 1170
- D’Antona, F. & Mazzitelli, I. 1997, in *Cool Stars in Clusters and Associations*, eds. R. Pallavicini & G. Micela, *Mem. S. A. It.*, 68, n.4.
- D’Antona, F. & Mazzitelli, I. 1998, *priv. comm.*
- de Geus, E. J. 1992, *A&A*, 262, 258

- de Zeeuw, P. T., Hoogerwerf, R., & de Bruijne, J. H. J., Brown, A. G. A., & Blaauw, A. 1999, *AJ*, 117, 354
- Dolidze, M. V. & Arakeylan, M. A. 1959, *Soviet-Astr.-AJ*, 3, 434
- Edwards, S., Cabrit, S., Strom, S., Heyer, I., Strom, K., & Anderson, E. 1987 *ApJ*, 321, 473
- Elias, J. H. 1978, *ApJ*, 224, 453
- Feigelson, E. D. 1996, *ApJ*, 468, 306
- Festin, L. 1998, *A&A*, 336, 883
- Gagné, M., Skinner, S. L., & Daniel, K. J. 2004, *astro-ph/0405467*
- Grasdalen, G. L. Strom, K. M., & Strom, S. E. 1973, *ApJ*, 184, L53
- Greene, T. P. & Meyer, M. R. 1995, *ApJ*, 450, 233
- Greene, T. P. & Young, E. T., 1992, *ApJ*, 395, 516
- Grosso, N., Montmerle, T., Bontemps, S., André, P., & Feigelson, E. D. 2000, *A&A*, 359, 113
- Hartigan, P. 1993, *AJ*, 105, 1511
- Hartmann, L., Hewett, R., & Calvet, N. 1994, *ApJ*, 426, 669
- Hawley, S. et al. 2002, *AJ*, 123, 3409
- Hillenbrand, L. A. 1997, *AJ*, 113, 1733
- Hillenbrand, L. A. & White, R. J. 2004, *ApJ*, 616, 998
- Imanishi, K., Koyama, K., & Tsuboi, Y. 2001, *ApJ*, 557, 747
- Kirkpatrick, J. D., Henry, T. J., & McCarthy, D. W. 1991, *ApJS*, 77, 417
- Lada, C. J. & Wilking, B. A. 1984, *AJ*, 287, 610
- Landolt, A. U. 1992, *AJ*, 104, 340
- Leous, J. A., Feigelson, E. D., André, P., & Montmerle, T. 1991, *ApJ*, 379, 683
- Loren, R. B. 1989, *ApJ*, 338, 925
- Livingston, W. C. 1999, in *Astrophysical Quantities* (4th Ed.), ed. A. Cox, (AIP Press: New York), p. 341
- Luhman, K. L. 1999, *ApJ*, 525, 466
- Luhman, K. L., Liebert, J., & Rieke, G. H. 1997, *ApJ*, 489, L165
- Luhman, K. L. & Rieke, G. H. 1999, *ApJ*, 525, 440
- Martín, E. L. 1997, *A&A*, 321, 492

- Martín, E. L., Montmerle, T., Gregorio-Hetem, J., & Casanova, S. 1998, *MNRAS*, 300, 733
- Montmerle, T., Koch-Miramonde, L., Falgarone, E., & Grindlay, J. E. 1983, *ApJ*, 269, 182
- Muzerolle, J., Calvet, N., & Hartmann, L. 2001, *ApJ*, 550, 944
- Natta, A., Testi, L., Comerón, F., D’Antona, F., Baffa, C., Comoretto, G., & Gennari, S. 2002, *A&A*, 393, 597
- Phelps, R. L. & Barsony, N. 2004, *AJ*, 127, 420
- Preibisch, T. & Zinnecker, H. 1999, *AJ*, 117, 2381
- Preibisch, T., Guenther, E., & Zinnecker, H. 2001, *AJ*, 121, 1040
- Preibisch, T., Brown, A. G. A., Bridges, T., Guenther, E., & Zinnecker, H. 2002, *AJ*, 124, 404
- Reipurth, B. & Clarke, C. 2001, *AJ*, 122, 432
- Reipurth, B., Pedrosa, A., & Lago, M. T. V. T. 1996, *Astronomy & Astrophysics Supplement*, 120, 229
- Rydgren, A. E. 1980, *AJ*, 85, 438
- Schmidt-Kaler, Th. 1982, in *Landolt-Bornstein New Series, Numerical Data and Functional Relationships in Science and Technology, Group 4, Vol. 2b*, edited by K. Schaffers and H. H. Voigt (Springer: New York), p. 451
- Sterzik, M. F. & Durisen, R. H. 1995, *A&A*, 304, L9
- Struve, O. & Rudkjöbing, M. 1949, *ApJ*, 109, 92
- Torres-Dodgen, A. V. & Weaver, W. B. 1993, *PASP*, 105, 693
- Vrba, F. J., Strom, S. E., Strom, K. M. 1976, *AJ*, 81, 958
- Vrba, F. J., Strom, S. E., Strom, K. M., & Grasdalen, G. L. 1975, *ApJ*, 197, 77
- Wiling, B. A., Greene, T. P., & Meyer, M. R. 1999, *AJ*, 117, 469
- Wiling, B. A. & Lada, C. J. 1983, *ApJ*, 274, 698
- Wiling, B. A., Lada, C. J., & Young, E. T. 1989, *ApJ*, 340, 823
- Wiling, B. A., Meyer, M. R., & Greene, T. P., 2005, in preparation
- Wiling, B. A., Schwartz, R. D., & Blackwell, J. H. 1987, *AJ*, 94, 106
- Wiling, B., Schwartz, R. D., Fanetti, T., & Friel, E. 1997, *PASP*, 109, 549

Figure Captions

Fig. 1.— A collection of spectra which is representative of the entire sample is presented, smoothed to a resolution of 5.73 \AA and normalized using a polynomial fit. The spectra are labeled with their field/aperture numbers (Table 2) and a spectral type or range. In addition, indicator of association membership (A) or undetermined (U) follows the spectral type. Atomic and molecular bands of interest in our classification scheme are labeled as well as telluric features. Fig. 1a shows B-G stars, Fig. 1b shows K stars, Fig. 1c the early M stars and Fig. 1d the late M stars. Included in Figs. 1c and 1d are spectra of giants and dwarfs from our survey to illustrate the intermediate surface gravity of the YSOs.

Fig. 2.— A plot of the spectral indices for dwarf standards used to guide our spectral classifications. Spectra from the studies of Allen & Strom (1995) or Kirkpatrick, Henry, & McCarthy (1991) were used in the analysis. Fig. 2a shows a plot of the TiO index of $7035\text{\AA}/7140\text{\AA}$ vs. the TiO index of $7500\text{\AA}/7800\text{\AA}$ for K5-M9 dwarfs. The ratios were formed by averaging the flux in a 30 \AA wide band centered on the wavelength. Fig. 2b plots the two VO band indices which are sensitive to spectral type for late M dwarf standard stars. Spectra from the studies of Allen & Strom (1995) or Kirkpatrick, Henry, & McCarthy (1991) were used in the analysis. The width of the wavelength bands in the continuum were chosen to maximize the number of channels yet avoid strong absorption due to TiO. The y-axis shows the ratio between the continuum averaged between a 20 \AA wide band centered at 7380 \AA and a 30 \AA wide band centered at 7555 \AA to the flux in a 50 \AA wide band centered in the VO band at 7465 \AA . The x-axis shows the ratio of the continuum in a 40 \AA wide band centered at 8120 \AA to the flux in a 60 \AA wide band centered in the VO band at 7970 \AA .

Fig. 3.— A plot of the CaH vs. TiO indices as defined in the text for 136 program objects. The solid lines were derived from first or second order fits to dwarf and giant spectral standards. For the dwarf standards from K5-M7, the fit was $y = 0.126x + 0.940$ with a correlation coefficient of $r=0.94$. We note that for spectral types later than M7, both indices decrease in response to an overall depression of the continuum so that an M8 V star has a CaH index similar to that of a M4 V star. For the giant standards from K5-M5, the fit gave $y = -0.0357x^2 + 0.191x + 0.795$ with a correlation coefficient of $r=0.82$.

Fig. 4.— The distribution of spectral types derived for 131 program objects. The bins were chosen to permit a direct comparison with similar histograms derived for other star-forming regions (e.g., Hillenbrand 1997). The shaded areas indicate objects which displayed strong H α emission $EW(\text{H}\alpha) > 10 \text{ \AA}$.

Fig. 5.— An expanded view of H α and Ca II emission lines in 7 CTTS labeled by their

field/aperture numbers (Table 2) and spectral types. The bottom two spectra are from the same source observed on two different nights. Fig. 5a shows the structure of the H α emission line with the rest wavelength of H α marked as a reference. Fig. 5b shows the Ca II triplet for the same objects.

Fig. 6.— The distribution of association members is shown relative to contours of ^{13}CO column density. The contours were computed from Loren (1989) assuming LTE and $T_{ex} = 25$ K. The values of the contours in units of cm^{-2} are 6×10^{14} , 3×10^{15} , and 1.5×10^{16} ; the lowest contour delineates the outer boundary of the dark cloud. The dashed box outlines the field included by our Hydra observations. Star symbols mark the locations of the star ρ Oph A (labeled) and the embedded association member Oph S1 in the L1688 core.

Fig. 7.— A Hertzsprung-Russell diagram for the ρ Oph association members with optically determined spectral types. The solid diamonds mark the positions of CTTS ($\text{EW}(\text{H}\alpha) > 10 \text{ \AA}$) and the open diamonds correspond to WTTS or post-T Tauri stars relative to the theoretical tracks of D’Antona & Mazzitelli (1997,1998). Isochrones shown as solid lines are 10^5 , 3×10^5 , 10^6 , 3×10^6 , 10^7 , and 10^8 years. Evolutionary tracks from $0.02 M_{\odot}$ to $2.0 M_{\odot}$ are shown by dashed lines. The bold dashed line marks the evolutionary track for a star at the hydrogen-burning limit. The typical error bar for a candidate is shown in the lower left of each plot and is ± 0.015 dex in $\text{Log}(T_{eff})$ and ± 0.12 dex in $\text{Log}(L_{bol}/L_{\odot})$.

FIGURE 1.A

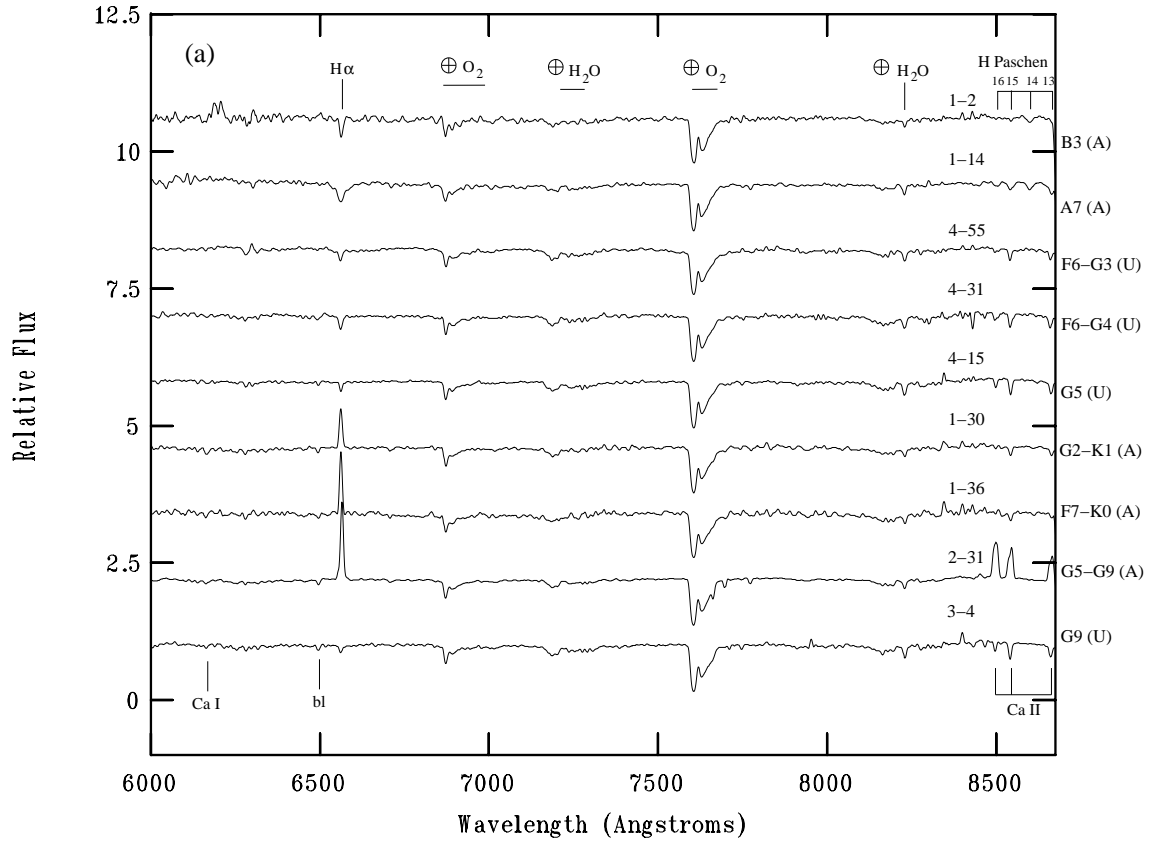


FIGURE 1.B

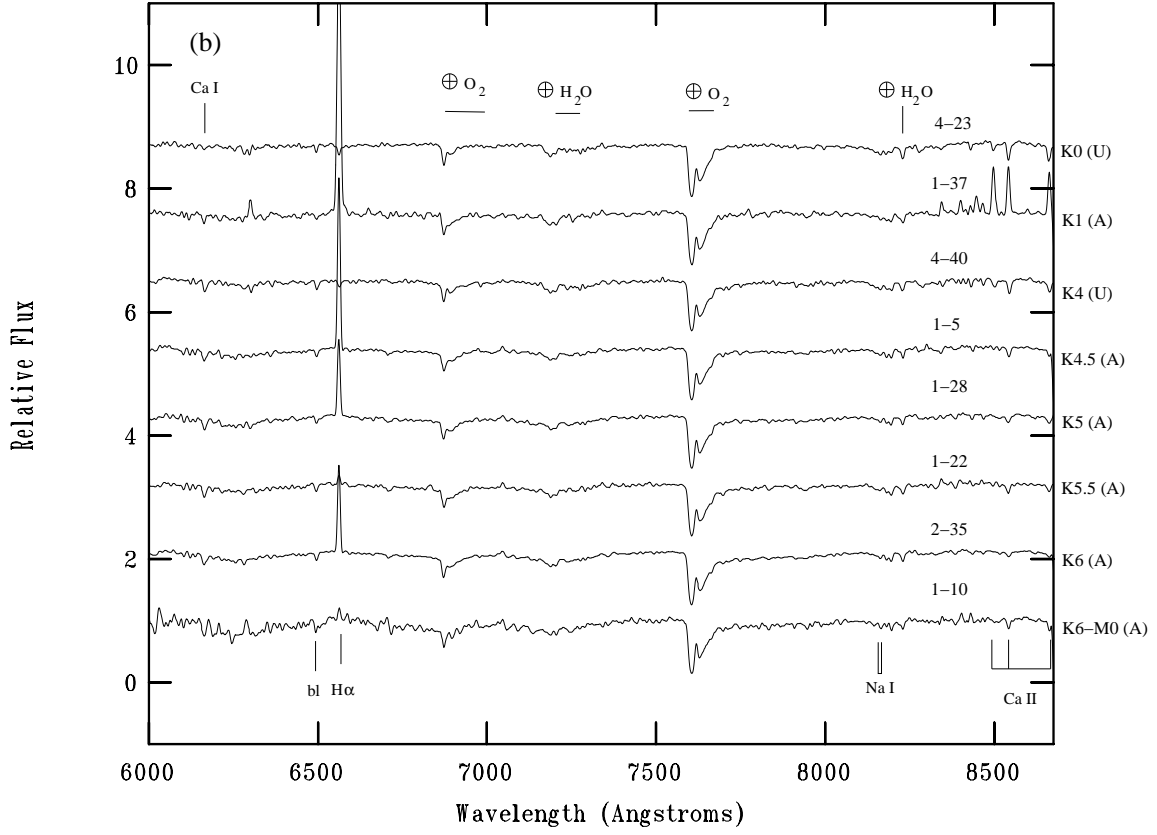


FIGURE 1.C

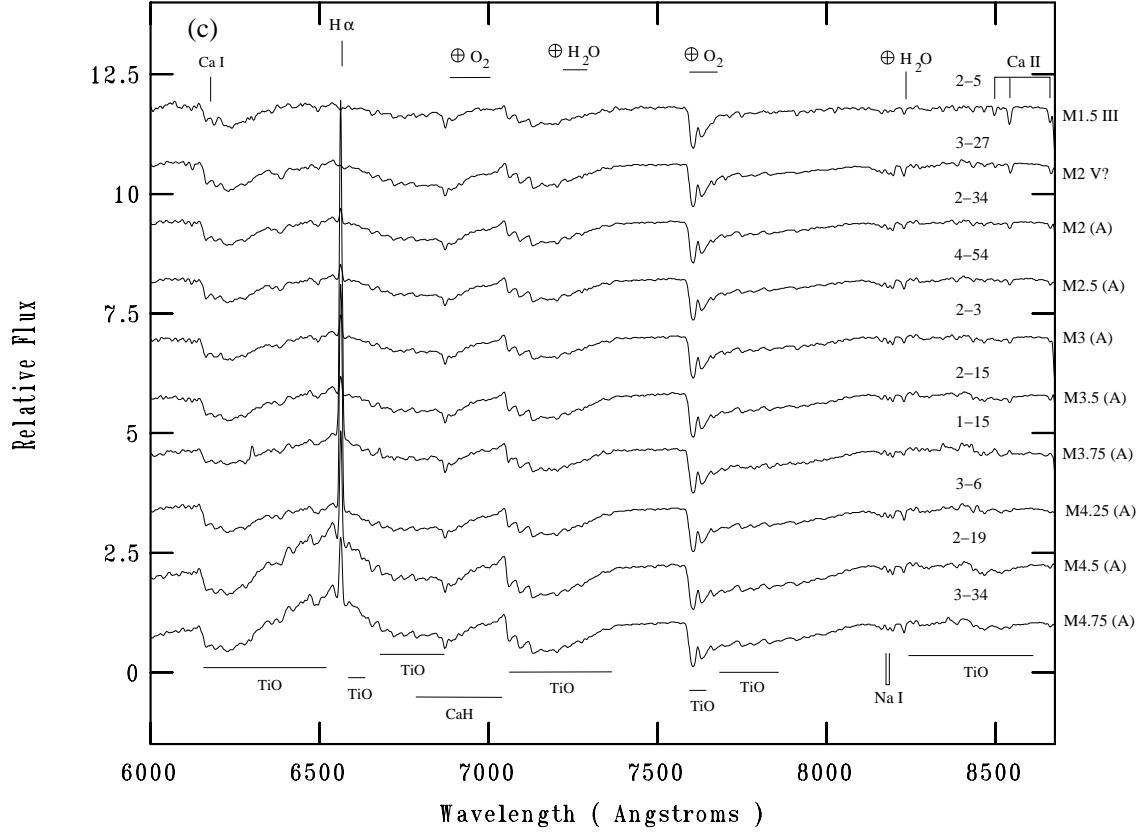


FIGURE 1.D

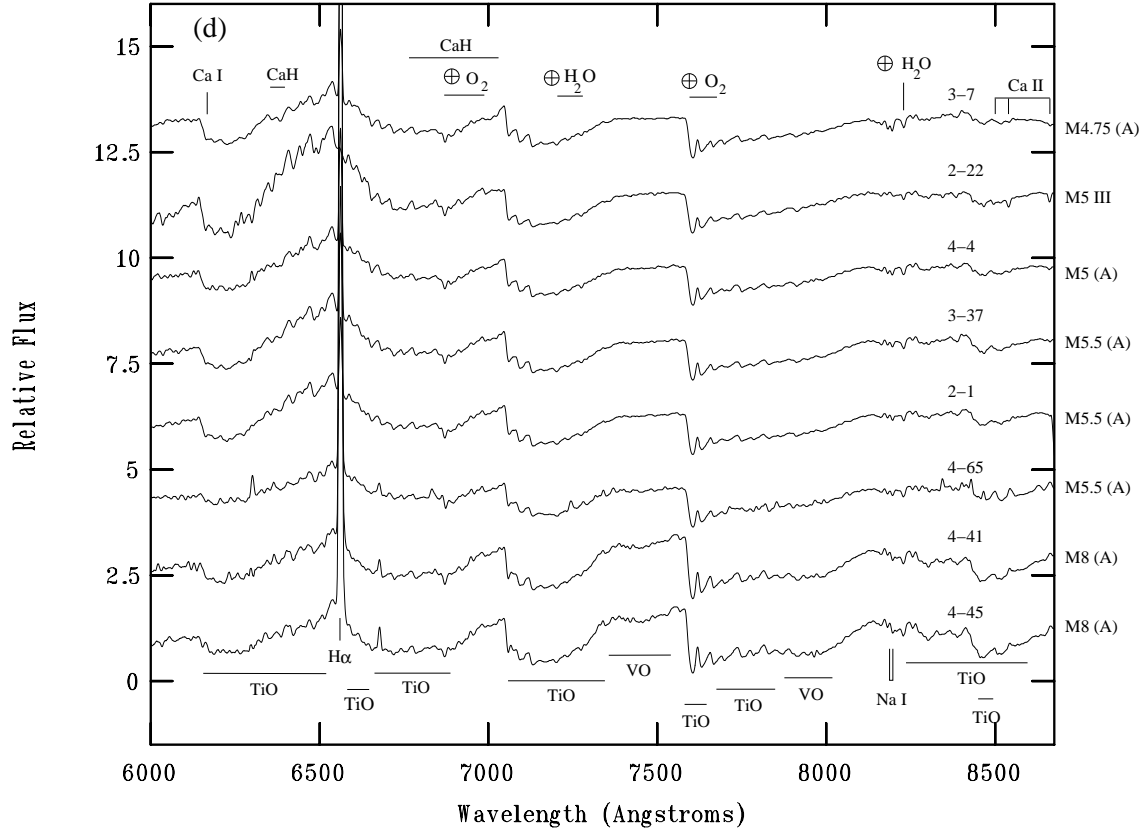


FIGURE 2.A

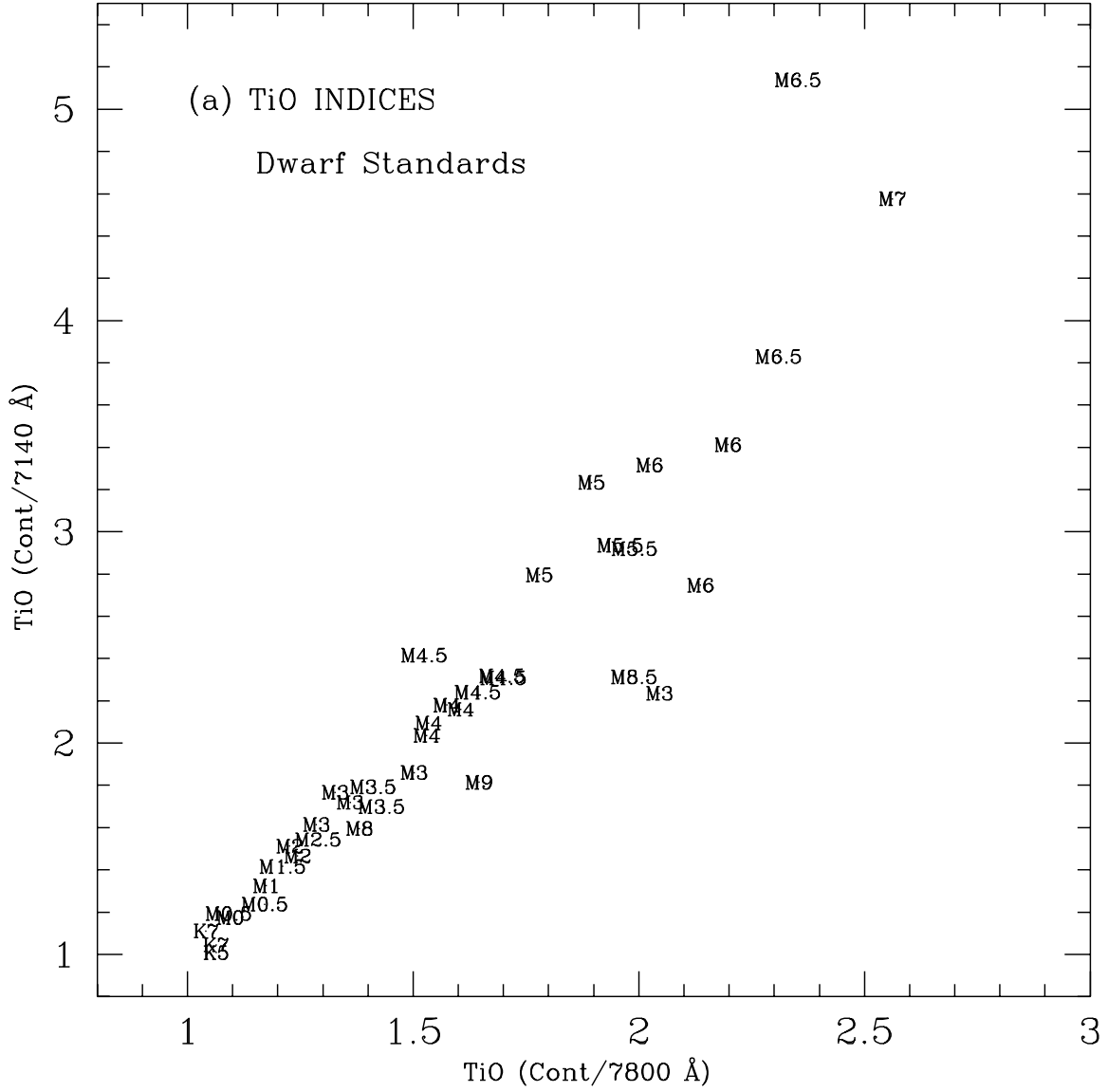


FIGURE 2.B

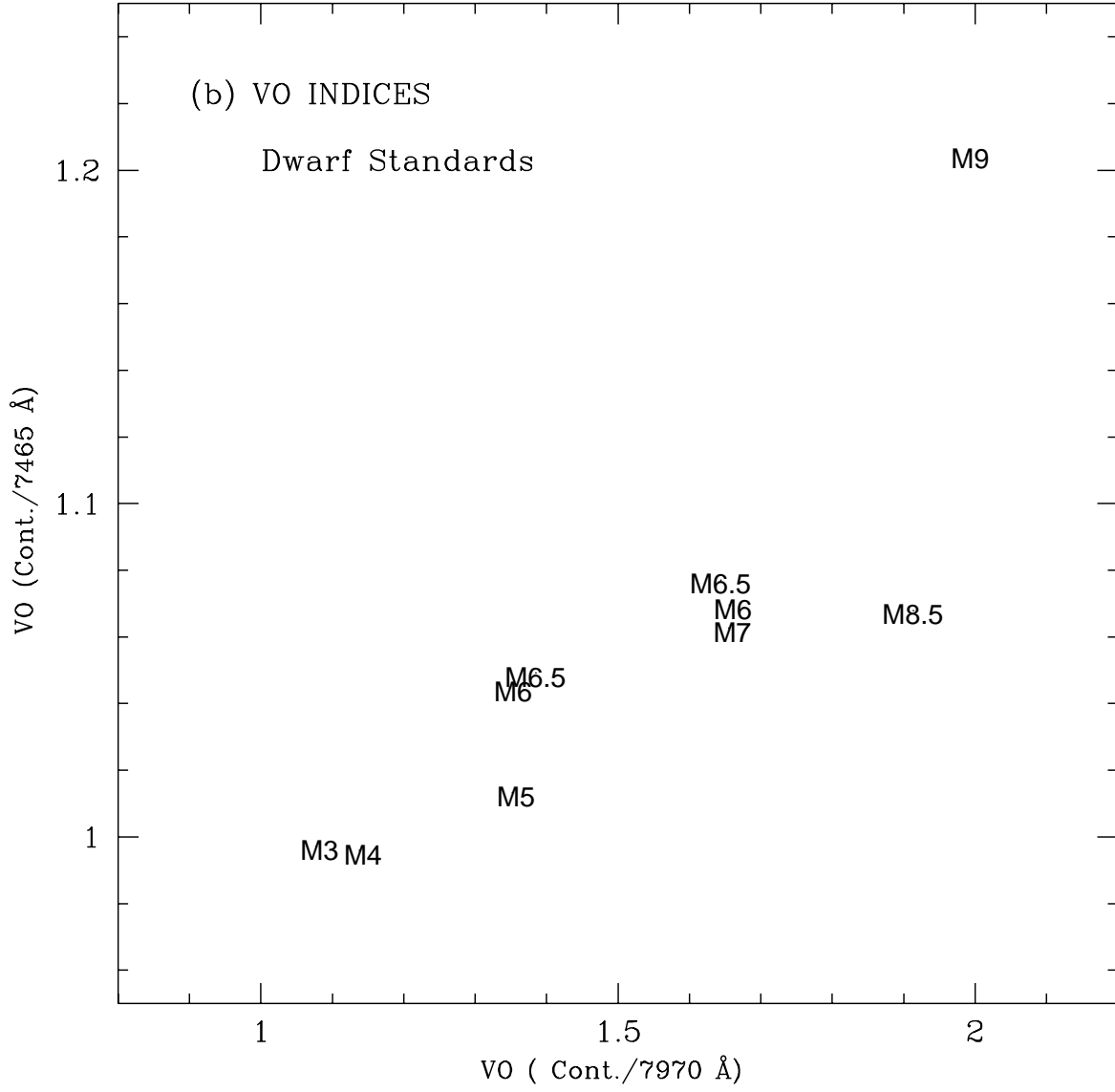


FIGURE 3

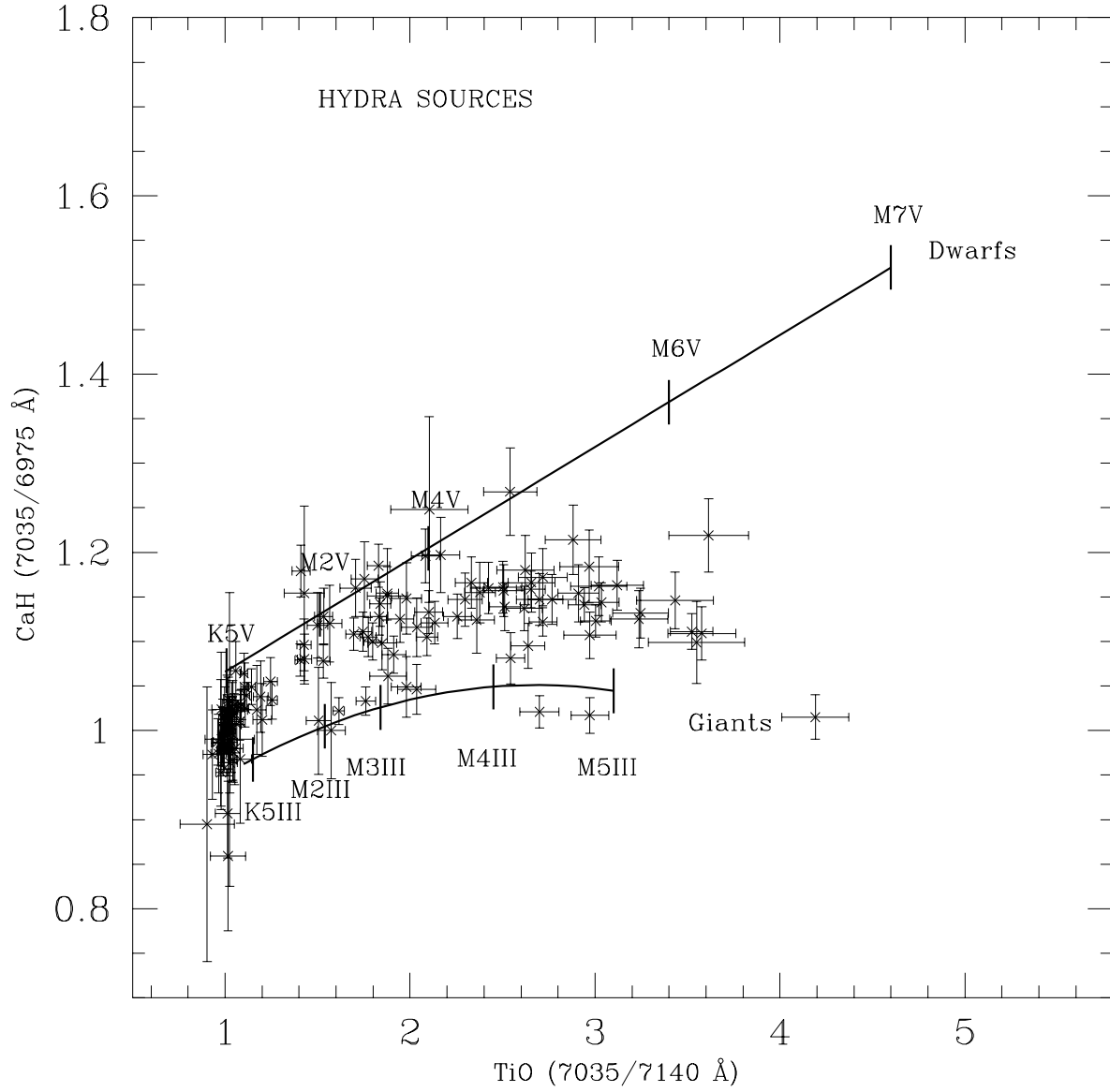


FIGURE 4

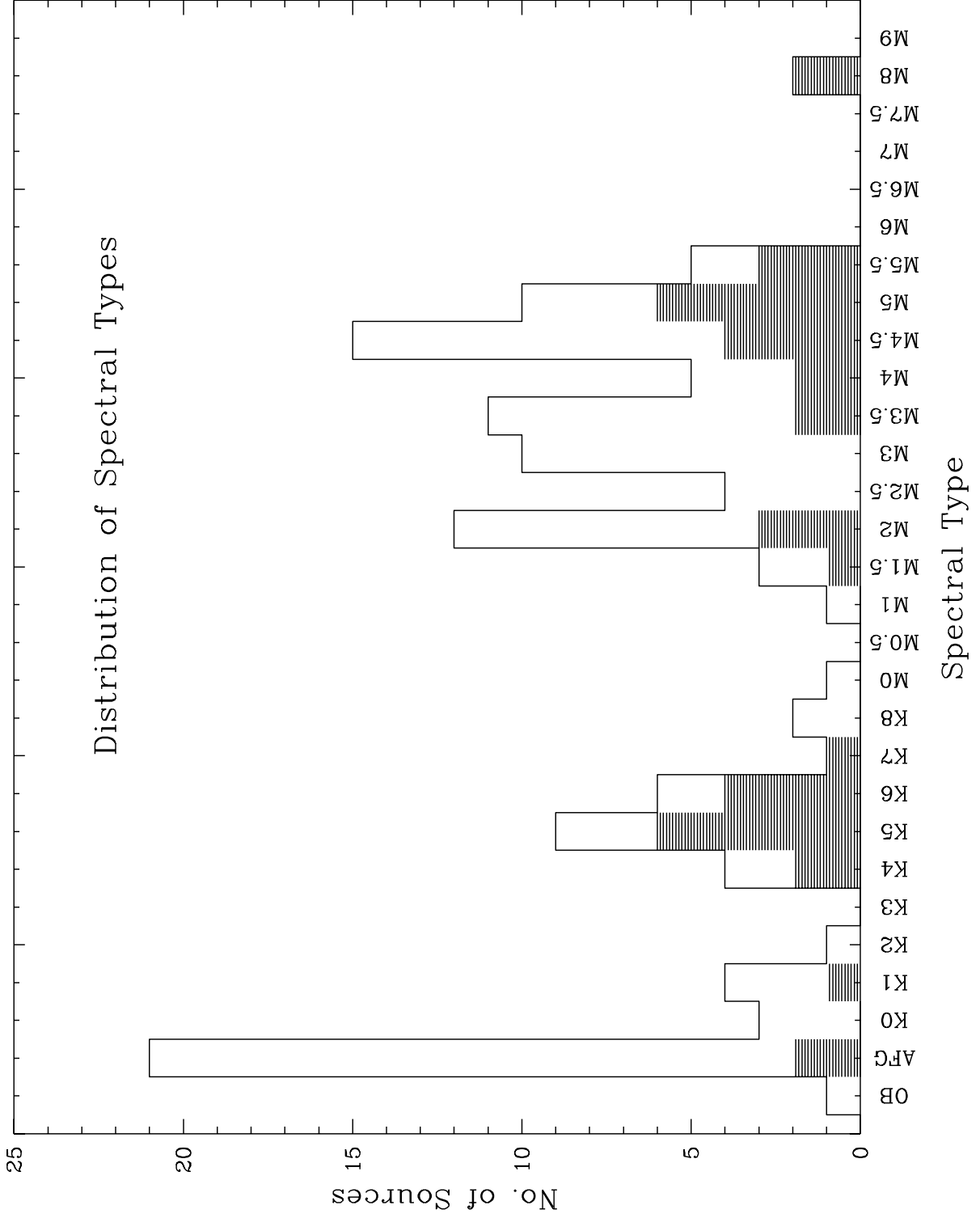


FIGURE 5.A

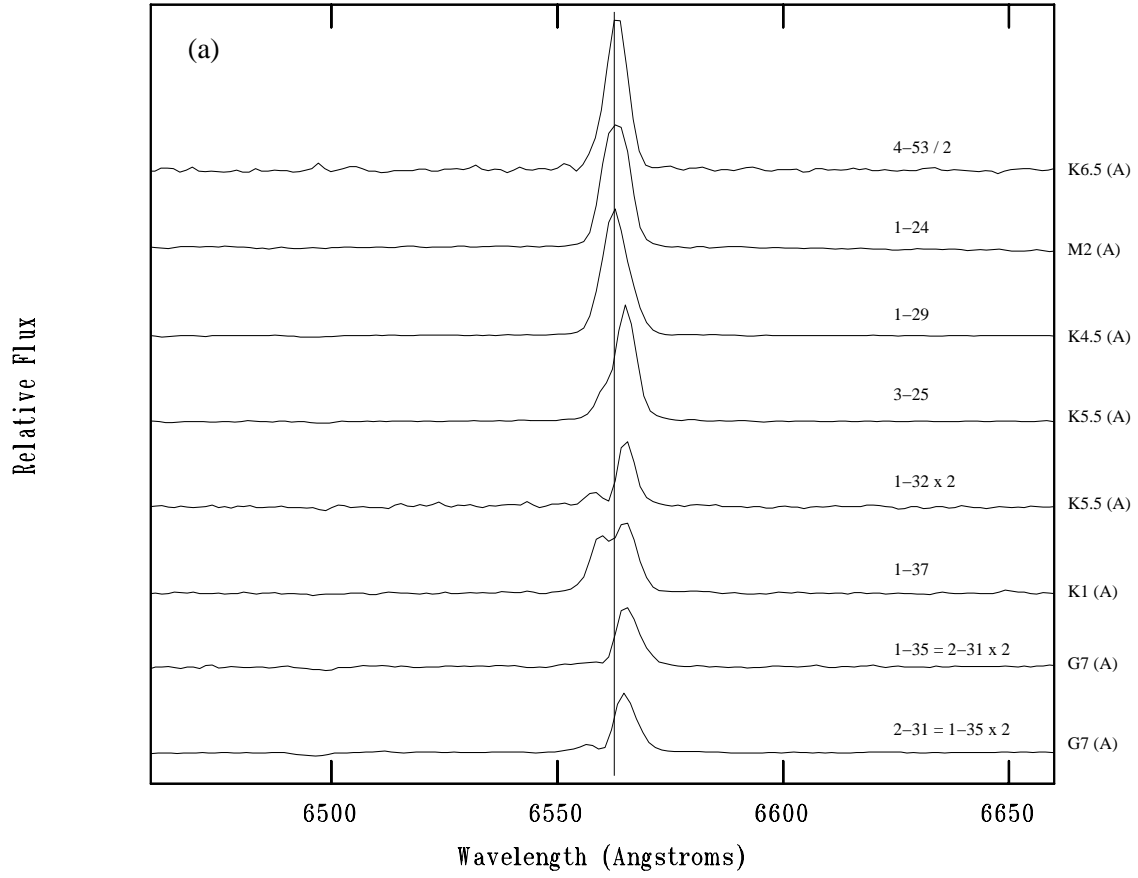


FIGURE 5.B

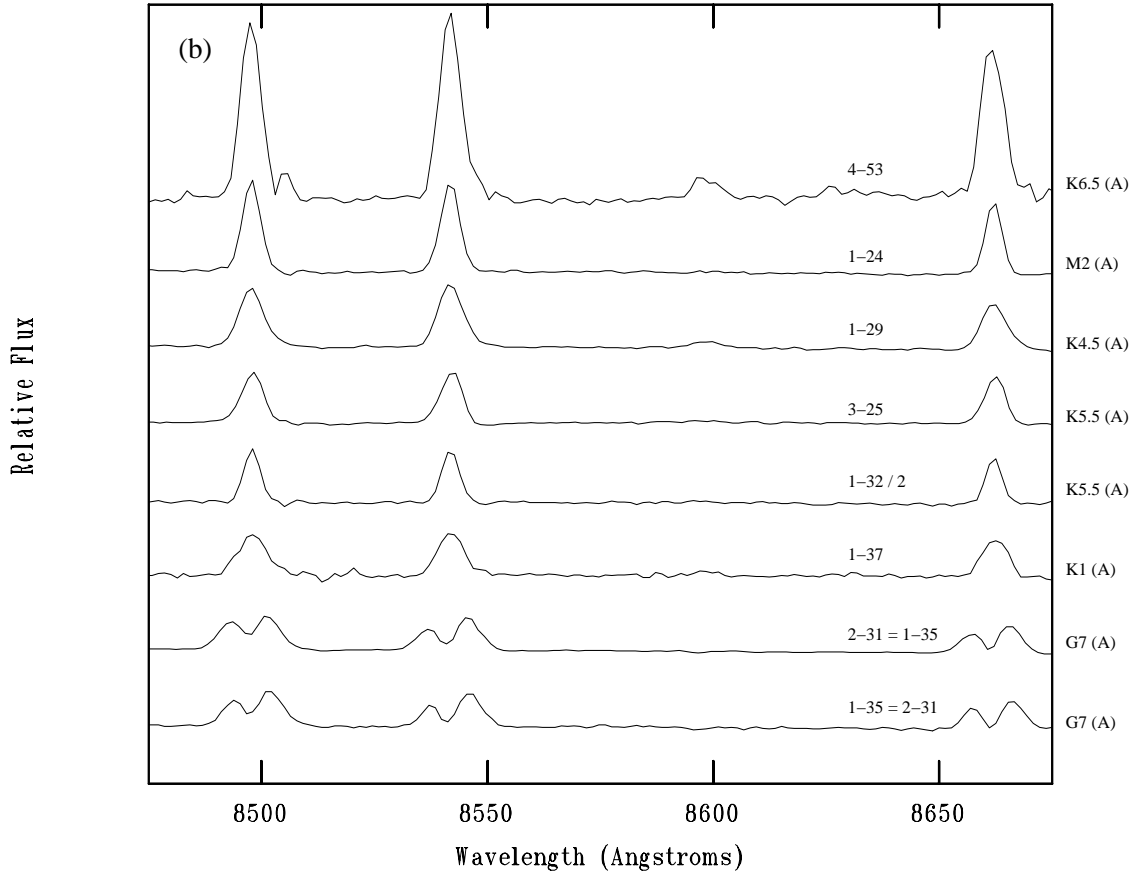
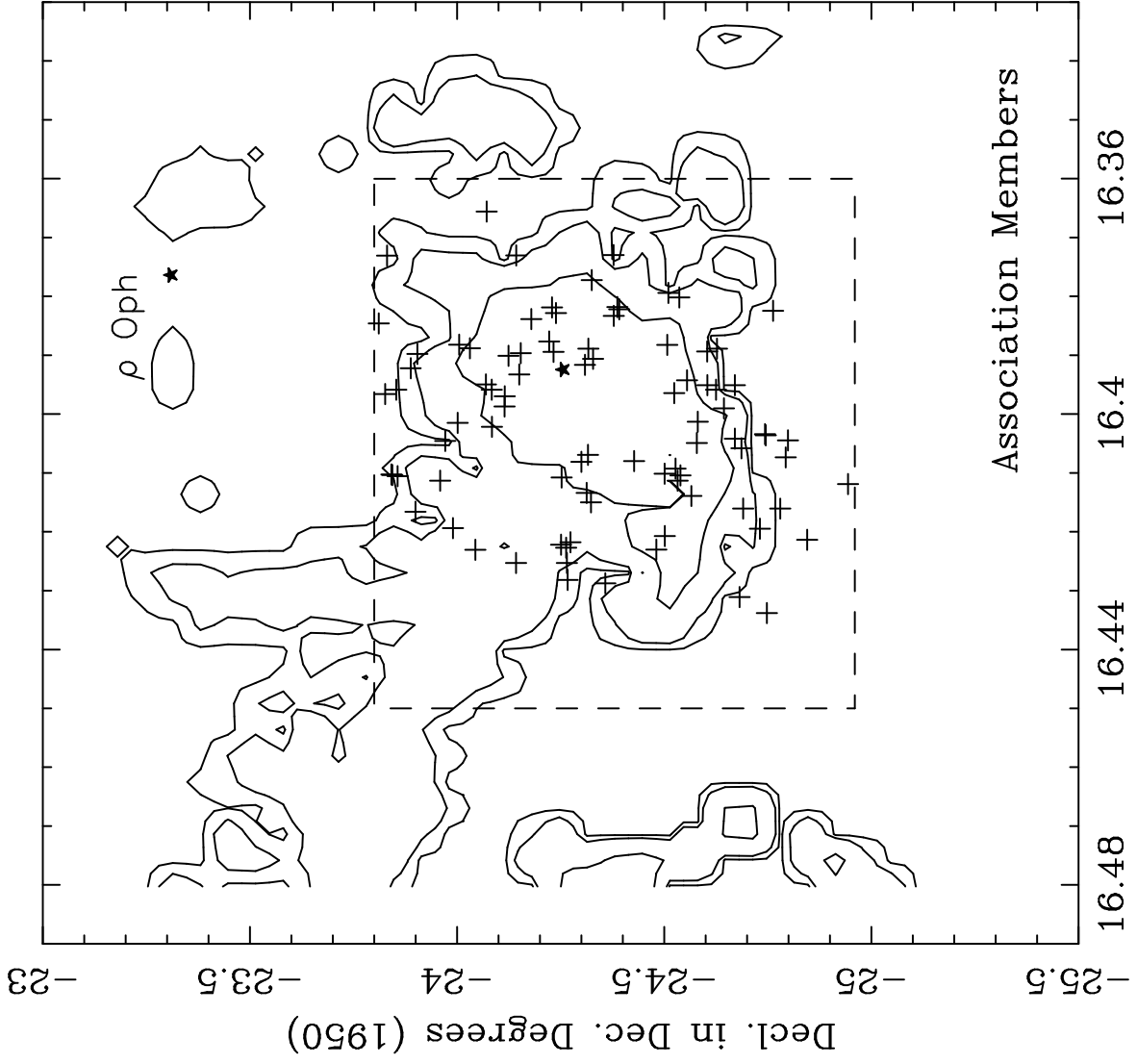


FIGURE 6



R. A. in Dec. Hours (1950)

FIGURE 7

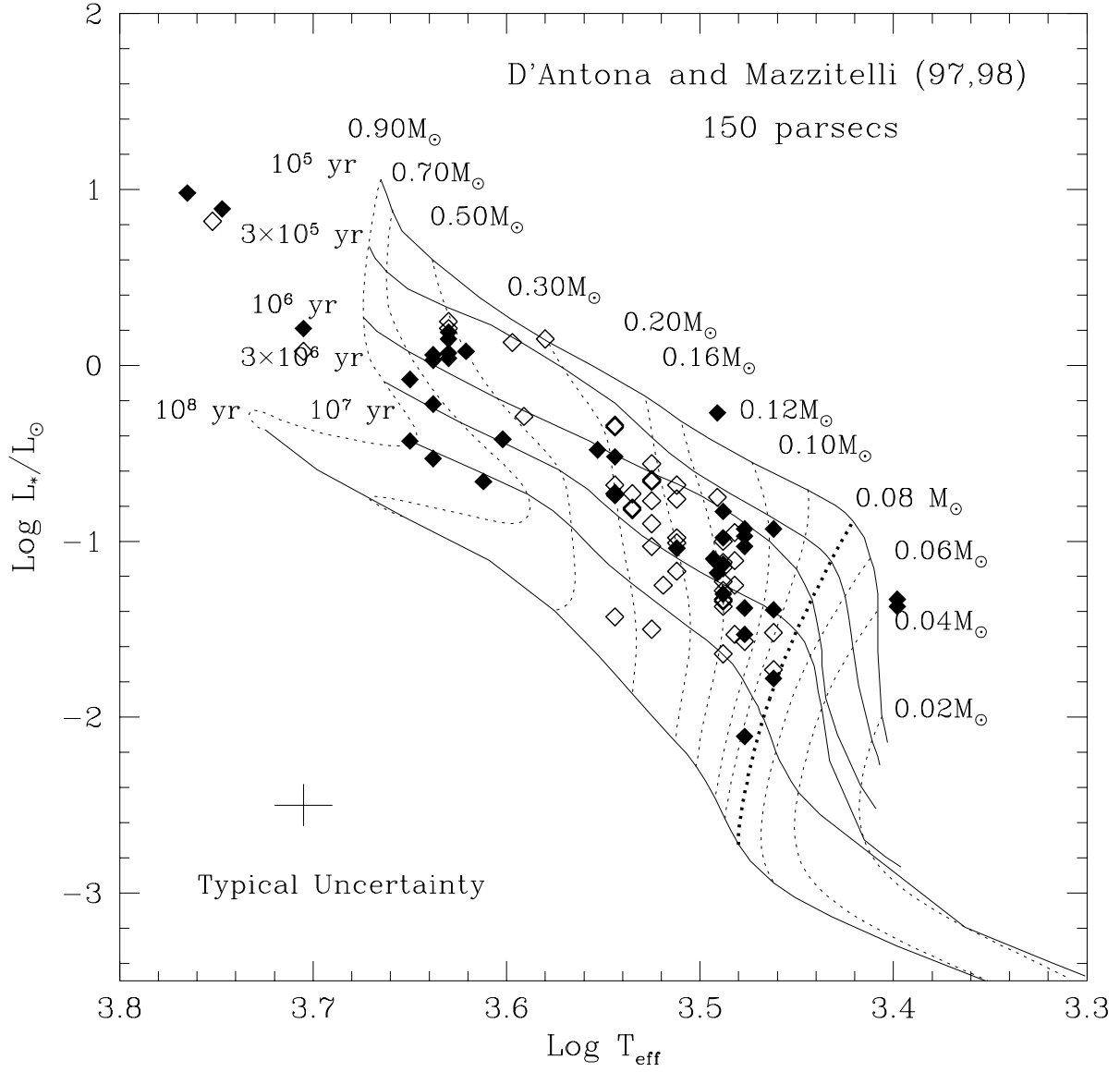


Table 1. Summary of Hydra Observations

Field No.	Position (J2000.0)	R (mag)	Sources Obs.	Int. Time (sec.)	No. of Exp.	\overline{SNR}^a
1	16:27:09.5 -24:25:43.5	R<15	28	600	4	21
2	16:26:46.2 -24:11:45.0	15<R<17	30	1800	4	21
3	16:27:19.9 -24:41:42.8	15<R<17	35	1800	2	23
4	16:27:18.3 -24:23:42.9	17<R<19.1	58	1800	4	16

^aMedian of signal-to-noise computed from 7400-7500 Å.

This is Table 2 of our HYDRA paper

TABLE 2
OPTICAL PROPERTIES OF CANDIDATE T TAURI STARS

F	Ap. ^a	Names(s) ^b	X-Ray ID ^c	RA(J2000) (hhmmss.s)	DEC(J2000) (° ' ")	CaH ^d	TiO ^e	EW(Li) (Å)	Prev. H α ^f (Å)	EW(H α) (Å)	I (mag)	(R-I) (mag)	Prev Sp. Ty. ^g	Sp. Ty.	Adopt	Notes
2	15			16 24 57.3	-24 11 23.4	1.10	2.09	yes	...	2.8	13.71	1.92	...	M3-4	M3.5	
2	22			16 25 01.5	-24 28 58.1	1.01	4.19	-0.10	13.85	2.42	...	M5	M5III	giant
2	14			16 25 24.1	-23 56 56.4	1.27	2.54	1.5	15.15	1.70	...	M2-4	M3	dwarf?
2	10			16 25 24.3	-24 15 39.0	1.22	3.61	11	14.46	2.03	...	M5	M5	
1	7	SR22,WSB23	ROXRA2	16 25 24.4	-24 29 43.5	1.18	2.62	...	170	31	12.88	1.64	M3.5(MMGC),M0(LR)	M4.5	M4.5	(h)
2	13			16 25 28.8	-24 22 59.0	1.20	2.17	0.30	15.12	1.52	...	M3-3.5	M3.25	dwarf?
3	27			16 25 29.9	-24 39 14.5	1.16	1.71	-0.10	14.15	1.22	...	M2	M2	dwarf?
4	43			16 25 31.6	-24 21 21.6	0.98	1.02	-0.50	17.02	1.62	...	K0-3	K1.5	
2	8			16 25 37.8	-24 13 43.1	1.02	2.97	yes:	...	0.40	13.56	2.47	...	M4-4.5	M4.25III	giant
3	15	WLY2-3	ROXRA4	16 25 39.6	-24 26 34.0	1.10	1.43	34	14.84	1.94	...	M2	M2	
2	32		ROXR1-7	16 25 47.7	-24 37 38.7	1.13	2.26	yes	4.9	4.7	14.25	1.92	M4(MMGC)	M3-4	M3.5	
1	22	VSS23,WLY2-10	ROXRA5	16 25 50.5	-24 39 13.9	1.03	1.08	yes:	2.5	1.2	12.37	1.45	K2(BA)	K5-6	K5.5	dwarf?
4	55			16 25 52.5	-24 04 18.7	1.02	1.01	-1.1	16.00	1.12	...	F6-G3	F9.5	
2	25	WLY2-11		16 25 56.1	-24 30 14.4	1.15	3.06	12	14.52	2.28	...	M5	M5	6cm ⁱ
3	18	same as above				1.14	3.02	14			...			
1	29	SR4,WSB25	ROXRA6	16 25 56.2	-24 20 47.5	1.03	1.05	yes	87/220	67	11.33	0.63	K6(BA),K8(LR)	K4-5	K4.5	Ca em
1	38	GSS20	ROXRA7	16 25 57.5	-24 30 30.9	0.98	1.05	...	1.5	0.50	13.00	1.59	K7(BA),K6(LR)	K5-6	K5.5	dwarf?
3	14			16 25 58.9	-24 52 47.4	1.17	2.72	yes	...	4.7	13.84	1.93	...	M4.5	M4.5	dwarf?
2	1	Chini8	ROXRA8	16 25 59.6	-24 21 21.6	1.12	3.50	yes	...	10	13.00	2.03	M4(LR)	M5.5	M5.5	
3	24	same as above				1.11	3.56	yes	...	10			...			
4	28		ROXRA9	16 26 01.6	-24 29 44.2	1.09	1.91	yes:	...	3.0	15.00	2.22	...	M3	M3	
1	13	VSSG19	ROXRA12	16 26 03.3	-24 17 46.0	1.17	1.75	...	2.1	2.1	12.99	1.71	M3(MMGC)	M2	M2	
2	19			16 26 05.5	-23 55 40.7	1.15	2.91	yes	...	11	13.75	2.10	...	M4.5	M4.5	
1	5	GSS28,WSB27	ROXRA15	16 26 17.1	-24 20 21.2	1.01	1.06	yes	20	29	11.84	1.00	K5(BA),M0(LR)	K4-5	K4.5	
4	39			16 26 18.7	-24 07 18.7	1.13	2.10	yes	...	2.3	13.06	1.80	...	M3-4	M3.5	
2	11		ROXR1-20	16 26 19.5	-24 37 26.8	1.15	2.97	yes	4.8	4.0	13.31	1.85	M4.5(MMGC)	M4.5-5	M4.75	
3	28	same as above				1.13	2.91	yes	...	5.0			...			
3	26			16 26 21.1	-25 03 47.9	2.7	U		R=16.21
1	25	WSB28	ROXRA16	16 26 21.0	-24 08 51.4	1.12	1.57	10	13.08	1.62	...	M2	M2	
4	16	GY5	ROXR1-C14	16 26 21.5	-24 26 00.4	1.10	3.55	15	15.80	2.50	M6(WGM),M6(N02)	M5.5	M5.5	
4	41	GY3	ROXR1-21	16 26 21.9	-24 44 39.4	1.11	2.97	140	15.62	2.33	M7.5(N02)	M8	M8	Ca em
4	40			16 26 22.5	-23 58 19.2	1.03	1.04	-0.70	16.09	1.34	...	K3-K5	K4	
1	30	GSS31,WSB30	ROXRA18	16 26 23.3	-24 20 59.1	1.00	1.01	...	5	7.1	11.75	1.28	K0(BA),K1(LR)	G2-K1	G6	
1	28	DoAr25,WSB29	ROXRF1	16 26 23.7	-24 43 13.3	1.03	1.11	yes	16	12	11.59	1.06	K7(MMGC),K6(LR)	K5	K5	
2	27	EL24,WSB31	ROXRA20	16 26 24.1	-24 16 13.0	1.02	1.05	yes:	...	44	13.97	1.84	...	K5-6	K5.5	Ca em
3	25	same as above				1.02	1.07	yes:	...	50			...			
4	18			16 26 24.3	-24 01 15.6	1.18	2.97	8.0	15.83	2.12	...	M4.5	M4.5	dwarf?
4	25		GDSJ162625.7	16 26 25.7	-24 14 27.1	1.15	3.43	7.2	15.79	2.27	...	M5.5	M5.5	
4	66	GY37	ROXR1-C15	16 26 27.9	-24 26 41.6	1.00	1.57	10	17.85	2.45	M6(WGM)	M4.5-5.5	M5	
4	31			16 26 29.2	-24 48 16.0	1.00	0.99	-2.7	16.45	1.06	...	F6-G4	G0	
4	27	GY59	GDSJ162631.3	16 26 31.4	-24 25 30.6	0.0	18.90	...	M5(LR),M6(WGM)	M2-M5.5	M3.75	
2	36	WSB34		16 26 33.0	-24 00 16.5	1.14	2.51	yes:	...	51	14.13	1.89	...	M4.5	M4.5	
1	2	Source1	ROXRA21	16 26 34.2	-24 23 27.8	1.02	1.04	...	-3.5	-2.6	12.57	1.95	B2(CK),B4:(BA)	<B8	B3	6cm ⁱ
4	4		ROXRA22	16 26 37.1	-24 15 59.4	1.16	3.12	yes:	...	14	15.51	2.21	...	M5	M5	
2	29	WSB37		16 26 41.3	-24 40 17.6	1.12	3.10	yes	...	22	13.37	2.04	M4(LR)	M5	M5	
3	3	same as above				1.12	2.90	yes	...	25			...			
4	11	GY107		16 26 42.5	-24 22 17.1	0.0	M3III(WGM)	U		
1	21			16 26 43.1	-24 11 09.1	1.01	1.20	0.70	13.30	1.53	...	K7-M0	K8	

TABLE 2—*Continued*

F	Ap. ^a	Names(s) ^b	X-Ray ID ^c	RA(J2000) (hhmmss.s)	DEC(J2000) (^o ' '')	CaH ^d	TiO ^e	EW(Li) (Å)	Prev. H α ^f (Å)	EW(H α) (Å)	I (mag)	(R-I) (mag)	Prev Sp. Ty. ^g	Sp. Ty.	Adopt	Notes
1	20	GY112	ROXRF2	16 26 44.3	-24 43 13.5	1.06	1.88	...	7.8	6.0	13.22	1.75	M3.5(MMGC)	M2-4	M3	
3	22			16 26 44.4	-24 47 13.3	1.16	2.51	yes	...	3.5	13.88	1.84	...	M4.5	M4.5	dwarf?
4	13			16 26 46.1	-23 58 10.1	1.16	2.42	yes	...	2.8	15.52	2.11	...	M2-4	M3	
1	36	WSB38	ROXRA24	16 26 46.5	-24 11 59.7	0.97	1.04	yes	19	10	12.37	1.53	G9:(BA),K8(LR)	F7-K0	G3.5	
4	30		ROXRF3	16 26 47.1	-24 44 29.1	1.15	2.70	yes	...	5.4	15.19	2.22	...	M4.5	M4.5	dwarf?
4	59			16 26 48.2	-24 42 03.2	1.05	1.98	1.0	15.56	2.25	...	M3-4.5	M3.75	
1	32	WSB40		16 26 48.6	-23 56 34.3	1.06	1.25	23	12.92	1.53	...	K5-6	K5.5	Ca em
4	53	WL18	ROXCH3	16 26 49.0	-24 38 24.8	0.97	1.08	96	17.38	1.95	...	K5-K8	K6.5	Ca em
2	38			16 26 50.5	-24 13 51.9	1.16	2.50	5.5	14.78	2.04	...	M4.5	M4.5	dwarf?
2	17			16 26 51.7	-24 03 53.9	1.02	2.70	0.10	13.11	2.36	...	M4	M4III	giant
4	32			16 26 53.2	-24 05 58.2	1.02	1.00	-1.9	16.88	1.52	...	G9-K2	K0.5	
2	9			16 26 55.0	-24 10 16.5	1.20	2.08	-0.40	13.81	1.47	...	M2-4	M3	dwarf?
4	46			16 26 56.7	-24 13 51.2	1.02	1.17	14	16.29	2.17	...	K5-M0	K7	
4	26			16 26 57.8	-24 52 37.1	0.98	1.04	-0.20	17.45	1.01	...	K5	K5	dwarf?
1	37	SR24s, WSB42	ROXRF7	16 26 58.5	-24 45 36.4	1.00	1.04	...	76	50	12.87	1.28	K7(MMGC),K2(LR)	K0-2	K1	Ca em
4	42			16 26 59.1	-23 56 39.0	0.99	0.98	0.50	15.95	1.26	...	U		
4	63			16 27 06.6	-24 07 02.9	1.15	2.77	5.7	15.34	2.19	...	M4.5	M4.5	dwarf?
4	65	GY204	ROXCH17	16 27 06.7	-24 41 48.8	1.08	2.54	43	15.43	2.14	M6(N02)	M5.5	M5.5	Ca em
4	37			16 27 09.1	-24 12 00.6	1.10	1.85	4.0	16.14	2.33	...	M2-3	M2.5	
3	44	ROX20a, WSB45		16 27 14.5	-24 51 33.4	1.17	2.33	yes	3	3.6	13.31	1.65	M5(BA),M1-4(LR)	M4.5	M4.5	dwarf?
1	9	ROX20b, WSB46	ROXRF14	16 27 15.1	-24 51 38.5	1.13	1.53	yes:	6.3	5.0	12.26	1.26	M2(BA),M0-3(LR)	M2	M2	dwarf?
3	17	WSB47		16 27 17.0	-24 47 10.9	1.01	1.08	-1.1	15.06	1.78	...	K0-2	K1	
4	10			16 27 17.5	-24 05 13.4	1.08	1.53	95	15.47	2.20	...	M3-4	M3.5	Ca em
4	9			16 27 18.1	-24 53 16.5	1.15	1.88	1.0	16.63	2.02	...	M2-3	M2.5	dwarf?
1	6	WSB48		16 27 18.4	-24 54 52.5	1.25	2.10	90	13.23	1.47	...	M3-4.5	M3.75	
...	...	SR12	ROXCH40	16 27 19.7	-24 41 39.9	4.5/8.8	...	11.10	1.30	K4/M2.5(BA),M0(LR)	...	M0	6cm ⁱ
4	62			16 27 20.4	-23 58 42.5	0.91	1.01	-0.20	17.42	1.31	...	U		
3	6	WSB49	ROXRF19	16 27 23.0	-24 48 06.8	1.12	2.13	yes	...	37	13.31	1.75	...	M4-4.5	M4.25	
4	45	GY264	ROXCH52	16 27 26.6	-24 25 54.2	1.12	3.24	155	15.72	2.18	...	M8	M8	Ca em
3	7		ROXRF24	16 27 28.8	-24 54 31.4	1.21	2.88	8.0	14.32	1.70	...	M4.5-5	M4.75	dwarf?
2	20		ROXR1-48	16 27 30.5	-24 32 34.7	1.19	1.83	-0.10	14.30	1.34	...	M2	M2	dwarf?
3	33	same as above				1.18	1.83	-0.20						
4	22	GY284	ROXR1-C27	16 27 30.9	-24 24 56.1	1.12	2.04	2.9	16.24	2.21	M1.5(LR)	M3-3.5	M3.25	
4	12			16 27 31.0	-24 03 44.1	0.99	1.02	-0.30	17.63	1.13	...	U		
1	19			16 27 31.3	-23 59 08.7	1.18	1.41	0.10	13.12	1.02	...	M1	M1	dwarf?
2	6	GY295, WSB50	ROXCH70	16 27 35.3	-24 38 33.4	1.14	2.77	yes	...	4.2	14.08	2.08	M4(LR)	M4.5	M4.5	
3	41	same as above				1.11	2.66	yes	...	4.0						
1	1	GY297		16 27 36.5	-24 28 33.3	1.12	1.50	-0.27	13.30	1.37	M0-3(LR)	M2	M2	dwarf?
4	54			16 27 38.0	-23 57 24.1	1.11	1.74	yes	...	3.0	13.71	1.74	...	M2-3	M2.5	
2	35	DoAr32, WSB51	ROX30b	16 27 38.3	-23 57 32.7	1.04	1.12	yes	22	13	12.30	1.36	K4(BA)	K5-7	K6	
4	24	WLY2-49	ROXRF29	16 27 38.3	-24 36 58.4	1.05	1.11	20	15.52	2.17	K8(LR)	K5-6	K5.5	
4	38	GY310		16 27 38.6	-24 38 38.4	0.79	1.70	0.0	17.40	...	M6(N02),M8.5(WGM)	M3-5	M4	
1	31	WSB53		16 27 39.0	-23 58 18.9	1.06	1.10	yes:	14	18	12.02	1.22	K4(BA)	K5-6	K5.5	
3	5	GY314, WSB52	ROXRF30	16 27 39.5	-24 39 15.6	1.05	1.14	yes	30	39	14.03	1.73	M0(LR, MMGC)	K5	K5	Ca em, 6cm ⁱ
1	26	SR9, WSB54	ROXRF31	16 27 40.3	-24 22 04.1	1.03	1.09	yes	10.5/14	23	11.26	0.50	K5(BA),K8(LR)	K5	K5	
2	34		RX1627.6-2404	16 27 41.8	-24 04 27.3	1.13	1.83	yes:	...	2.5	13.39	1.82	...	M2	M2	dwarf?
4	64	GY326	ROXCH81	16 27 42.7	-24 38 51.0	1.01	1.51	0.20	17.30	...	M4(WGM)	M2	M2	
3	21			16 27 45.2	-25 03 32.7	1.17	2.66	yes	...	3.5	14.09	1.83	...	M4.5	M4.5	dwarf?

TABLE 2—*Continued*

F	Ap. ^a	Names(s) ^b	X-Ray ID ^c	RA(J2000) (hhmmss.s)	DEC(J2000) (^o ['] ["])	CaH ^d	TiO ^e	EW(Li) (Å)	Prev. H α ^f (Å)	EW(H α) (Å)	I (mag)	(R-I) (mag)	Prev Sp. Ty. ^g	Sp. Ty.	Adopt	Notes
4	47			16 27 49.3	-23 56 09.0	1.02	1.01	0.0	16.48	1.06	...	F6-G9	G2.5	
1	14	VSSG14	ROXR1-53	16 27 49.9	-24 25 40.3	0.98	0.98	...	-9.1	-8.0	12.19	1.50	A7(GM,MMGC)	<F1	A7	6cm ⁱ
1	10	ROX31	ROXRF33	16 27 52.1	-24 40 50.3	1.04	1.19	...	3.3	1.3	12.66	1.60	K7(BA)	K6-M0	K7.5	6cm ⁱ
1	24	SR10,WSB57	ROXR1-C12	16 27 55.6	-24 26 18.0	1.11	1.70	yes:	43	56	11.95	1.18	M1.5(CK),M0(LR)	M2	M2	Ca em
4	8			16 27 59.7	-23 57 16.5	1.15	1.43	0.60	16.99	1.76	...	M0	M0	
3	34	WSB58	ROXRF34	16 28 00.0	-24 48 19.3	1.14	2.62	yes:	...	7.5	13.40	1.98	...	M4.5-5	M4.75	
3	31		ROXRF35	16 28 00.1	-24 53 42.5	1.13	3.25	yes	...	14	13.51	2.05	...	M5	M5	
2	3			16 28 00.8	-24 00 52.0	1.10	1.77	yes	...	3.2	13.89	1.85	...	M2-4	M3	
4	61			16 28 04.9	-23 56 08.4	0.97	0.97	-0.10	17.26	1.23	...	K5	K5	
4	5			16 28 09.9	-24 48 47.5	1.00	1.03	-0.80	16.66	0.88	...	K4-5	K4.5	
2	21			16 28 11.1	-24 06 17.9	1.16	2.38	yes:	...	7.7	14.27	2.13	...	M3-4.5	M3.75	
3	13			16 28 11.3	-24 59 05.8	1.02	0.99	-1.5	15.90	1.00	...	G5-G9	G7	
3	11		ROXRF36	16 28 12.4	-24 50 44.9	1.15	1.88	yes	...	6.0	13.67	1.93	...	M2-4	M3	dwarf?
4	51			16 28 14.4	-23 57 52.1	1.01	1.01	0.0	17.49	1.18	...	G5-9	G7	
3	9			16 28 15.1	-25 02 07.3	1.03	1.02	-1.5	15.32	0.92	...	G9-K0	G9.5	
3	19			16 28 15.6	-25 03 49.5	1.00	1.02	-0.40	15.53	0.47	...	G9-K1	K0	
3	20	WSB60		16 28 16.6	-24 36 58.3	1.09	2.64	yes:	...	81	14.46	2.09	K8(LR)	M4.5	M4.5	Ca em
4	58			16 28 16.6	-24 07 36.4	1.07	1.06	0.0	16.77	1.69	...	U		
4	14			16 28 18.1	-23 57 30.4	1.00	1.01	-1.5	16.57	1.08	...	F6-G4	G0	
3	12			16 28 19.2	-24 57 34.2	1.15	1.98	yes:	...	4.9	13.54	1.67	...	M2-4	M3	dwarf?
2	12			16 28 20.0	-24 26 10.9	0.97	0.93	-0.80	15.69	1.21	...	F9-G9	G5	
4	3			16 28 20.1	-24 23 17.8	1.15	2.30	yes:	...	4.1	15.55	2.14	...	M3-4	M3.5	
2	37			16 28 21.6	-24 21 55.2	1.14	1.48	1.0	14.95	2.02	...	M2-3	M2.5	
3	35	same as above				1.14	1.84	yes:	...	3.0			...			
2	5			16 28 23.3	-24 18 34.3	1.03	1.59	-0.80	14.38	2.04	...	M1-2	M1.5III	giant
3	29	same as above				1.02	1.65	-1.0			...			
2	30			16 28 23.4	-24 22 40.6	1.03	1.02	35	14.60	1.69	...	K5	K5	var H α
3	42	same as above				1.02	1.05	yes:	...	8.5			...			
2	4			16 28 24.3	-24 09 31.9	1.08	1.43	2.4	14.60	1.92	...	M2	M2	dwarf?
3	39			16 28 24.9	-24 35 43.4	1.16	3.02	yes	...	6.0	14.79	1.99	...	M5	M5	
1	11			16 28 25.1	-24 28 20.1	1.05	2.04	-0.50	12.46	1.79	...	M2	M2III	giant
4	44			16 28 28.3	-23 58 51.0	0.90	0.90	-0.20	17.17	1.20	...	U		
3	2			16 28 28.3	-24 52 21.6	1.03	1.26	-0.80	15.05	1.35	...	K6	K6	
4	23			16 28 29.4	-24 31 20.9	0.99	0.99	-0.90	16.56	1.22	...	K0	K0	
4	57			16 28 32.6	-24 15 24.1	1.12	2.36	4.0	15.95	2.35	...	M3-4	M3.5	
1	35	SR20,WSB61	ROX33	16 28 32.7	-24 22 45.2	1.00	1.00	yes:	21	15	11.36	1.23	G0:(BA),K8(LR)	G5-9	G7	db Ca em
2	31	same as above				1.00	1.00	yes:	...	15			...			
4	50			16 28 36.3	-24 00 43.2	0.99	1.00	-1.2	16.28	1.57	...	K0-2	K1	
2	23			16 28 43.1	-24 22 52.3	1.16	2.62	6.4	14.47	2.07	...	M4.5-5	M4.75	(j)
3	1	same as above				1.16	2.69	yes	...	6.0			...			
4	1			16 28 43.6	-24 04 44.7	1.00	0.99	-2.5	15.75	1.27	...	F7-G3	G0	
1	15	SR13,WSB62	ROX34	16 28 45.3	-24 28 19.0	1.10	1.80	yes:	30/48	46	10.95	1.45	M2.5(BA)	M3-4.5	M3.75	Ca em
4	49			16 28 47.0	-24 32 52.6	0.98	1.00	-1.20	16.85	1.10	...	G5-9	G7	
3	43	WSB63		16 28 54.1	-24 47 44.7	1.08	1.41	yes	...	50	13.54	1.70	...	M1-2	M1.5	
4	56			16 28 59.2	-24 05 15.6	0.95	0.98	-1.9	17.04	0.78	...	F6-G9	G2.5	
3	4			16 29 00.0	-24 26 39.2	1.01	1.00	-1.1	15.20	1.00	...	G9	G9	
4	52			16 29 02.0	-24 31 10.7	0.98	0.99	-0.90	17.39	0.91	...	G5-K0	G7.5	
4	35			16 29 03.8	-24 30 2.4	1.13	1.95	-0.50	16.54	1.71	...	M2-4	M3	dwarf?

TABLE 2—*Continued*

F	Ap. ^a	Names(s) ^b	X-Ray ID ^c	RA(J2000) (hhmmss.s)	DEC(J2000) (° ' ")	CaH ^d	TiO ^e	EW(Li) (Å)	Prev. H α ^f (Å)	EW(H α) (Å)	I (mag)	(R-I) (mag)	Prev Sp. Ty. ^g	Sp. Ty.	Adopt	Notes
3	37			16 29 04.0	-24 51 42.0	1.11	3.58	yes	...	9.0	14.49	2.04	...	M5.5	M5.5	
4	20			16 29 11.6	-24 22 14.8	0.99	1.03	-1.1	17.80	1.09	...	F6-G5	G0.5	
1	3			16 29 12.7	-24 23 55.8	1.03	1.76	-1.1	11.68	M1-2	M1.5III	giant
4	60			16 29 21.1	-24 21 32.2	0.86	1.02	-0.10	17.70	0.96	...	U		
4	21			16 29 23.5	-24 27 51.2	0.98	0.99	-1.4	17.48	0.87	...	K0-2	K1	
4	15			16 29 23.9	-24 29 10.8	0.99	0.98	-1.4	16.11	1.02	...	G5	G5	
4	2			16 29 24.5	-24 30 54.8	0.96	1.03	1.0	17.67	0.87	...	F6-G9	G2.5	
4	36			16 29 27.7	-24 24 39.0	0.99	0.96	-1.5	17.45	0.78	...	F6-G0	F8	

^aHYDRA field and aperture number of observation.

^bSources names from optical or infrared studies by: Struve & Rudkjøbing (SR, 1949); Dolidze & Arakelyan (DoAr, 1959); Grasdalen, Strom, & Strom (GSS, Source 1, 1973); Vrba *et al.* (VSSG, 1975); Vrba, Strom, & Strom (VSS, 1976); Elias (EL, 1978); Chini (1981); Wilking & Lada (WL, 1983); Montmerle *et al.* (ROX, 1983); Wilking, Schwartz, & Blackwell (WSB, 1987); Wilking, Lada, & Young (WLY, 1989); Greene & Young (GY, 1992).

^cX-ray source association from the EINSTEIN survey by Montmerle *et al.* (ROX, 1983), the ROSAT survey by Casanova *et al.* (ROXR1, 1996) and Grosso *et al.* (ROXRA or ROXRF, 2000), or the Chandra survey by Imanishi, Koyama, & Tsuboi (ROXCH, 2001) or Gagné, Skinner, & Daniel (GDS, 2004).

^dCaH index calculated from the ratio of flux from the center of the continuum at 7035 Å to the center of the CaH absorption at 6975 Å.

^eTiO index calculated from the ratio of flux from the center of the continuum at 7035 Å to the center of the TiO band at 7140 Å.

^fPreviously reported equivalent width of H α by Cohen & Kuhi (1979), Bouvier & Appenzeller (1992), or Martín *et al.* (1998)

^gReferences for spectral types: Cohen & Kuhi (CK, 1979); Bouvier & Appenzeller (BA, 1992); Greene & Meyer (GM, 1995); Martín *et al.* (MMGC, 1998); Luhman & Rieke (LR, 1999); Wilking, Greene, & Meyer (WGM, 1999); Natta *et al.* (N02, 2002)

^hR and I band photometry from Gordon & K. Strom, unpublished observations.

ⁱRadio continuum source at $\lambda=6$ cm observed by André. Montmerle, & Feigelson, E. (1987), Leous *et al.* (1991), or Gagné, Skinner, & Daniel (2004).

^jSNR in 6700 Å region too low to detect Li absorption

This is Table 3 of our HYDRA paper

TABLE 3
GAUSSIAN FITS TO EMISSION LINES OF T TAURI STARS

F	Ap. ^a	Names(s) ^b	He I ^c (5876Å)		[O II] ^d (6300Å)		H α ^e (6563Å)		Type	He I (6678Å)		He I (7066Å)		O I (7773Å)		O I (8447Å)		Ca II (8498Å)		Ca II (8542Å)		Pa 14 (8598Å)		Ca II (8662Å)			
			W λ	Δv	W λ	Δv	W λ	Δv		W λ	Δv	W λ	Δv	W λ	Δv	W λ	Δv	W λ	Δv	W λ	Δv	W λ	Δv	W λ	Δv	W λ	Δv
			(Å)	(km/s)	(Å)	(km/s)	(Å)	(km/s)		(Å)	(km/s)	(Å)	(km/s)	(Å)	(km/s)	(Å)	(km/s)	(Å)	(km/s)	(Å)	(km/s)	(Å)	(km/s)	(Å)	(km/s)	(Å)	(km/s)
2	10		14	180	I	
1	7	SR 22	3.0:	95	35	220	I	
3	15	IRS 3	34	260	I	0.64:	135	
2	25		13	300	IIR	
3	18	same as 2-25	16	360	IIR	
1	29	SR 4	3.3	300	70	320	I	0.73:	480	0.37:	130	1.4	290	2.8	290	10	220	11	230	1.4:	260:	9.6	230		
2	1	Chini 8	9.6	160	I	
3	24	same as 2-1	>13	170	IIB	
2	19		13	160	I	
1	5	GSS 28	27	240	I	
1	25	WSB 28	11	290	I	
4	16	GY 5	20	190	I	
4	41	GY 3	20:	230	>160	210	Iw	4.1	170	0.69:	80	0.71:	150	1.0	120	0.82	190	
1	28	DoAr 25	12	250	I	
2	27	EL 24	2.8:	240	>48	240	Iw	0.75:	160	0.36:	100	0.28:	140	1.6	240	4.5	180	5.0	160	4.4	150	
3	25	same as 2-27	1.7U	200	>53	280	IIIB	0.39U	150	0.33:	110	0.91	260	2.0	220	7.7	200	8.1	190	7.3	180	
4	66	GY 37	9.9	210	I	
2	36	WSB 34	5.7	180	56	240	I	1.9	170	0.75	150	1.4	310	
4	4		15	150	I	
2	29	WSB 37	1.4U	170	23	250	I	0.44U	160	0.30U	150	
3	3	same as 2-29	4.0:	160	28	270	I	1.1:	150	0.52:	140	
1	36	WSB 38	12	260	I	
1	32	WSB 40	>27	210	IIIB	1.4:	330:	3.5	150	12.8	140	13.5	160	12	140	
4	53	WL 18	130	260	IIIB	2.7:	130	3.2	140	28	180	33	200	3.9 ^f	230	24	190		
4	46		17	310	I	
1	37	SR 24s	3.0	230	>52	470	IIB	0.87:	220	3.8	320	8.3	260	8.4	240	1.0U	240U	7.3	220		
4	65	GY 204	2.8:	170	6.2	280	42	260	I	2.2:	220	0.54U	110	4.1	600	3.2	480	1.8	290	
4	10		11	160	2.9	100	100	230	Iw	3.4	120	1.4	100	2.2	220	2.9	140	2.6	140	3.1	130	2.5	130	
1	6	WSB 48	120	260	I	
3	6	WSB 49	1.9:	140	40	200	I	0.58:	120	0.36U	170	0.84:	130	
4	45	GY 264	24	160	>210	200	Iw	5.9	140	1.9	120	1.2:	150	1.3	120	0.65	90	
2	35	WSB 51	13	240	I	
4	24	IRS 49	20	230	I	
1	31	WSB 53	20	210	IIIB	
3	5	WSB 52	42	310	I	0.52	270	1.7	220	1.5	150	1.8	120	1.5	150	
1	26	SR 9	24	260	I	
1	24	SR 10	2.9	160	62	310	I	1.4	150	0.26U	90	1.0:	280	2.0	210	12	160	13	170	9.7	140	
3	31		14	160	I	
3	20	WSB 60	7.8	160	3.0	95	95	230	I	1.3	120	0.54	100	3.5	140	3.8	140	2.6	130	
2	30		40	320	I	
3	42	same as 2-30	>10	420	IIR	
1	35	SR 20	>16	270	IIIB	10	^g	8.6	^g	7.0	^g	
2	31	same as 1-35	>15	260	IIIB	10	^g	8.7	^g	7.8	^g	
1	15	SR 13	3.7	150	2.6	160	>50	200	Iw	1.4	110	0.60:	100	0.48U	160	0.6	110	0.81:	100	0.46U	90	
3	43	WSB 63	60	320	I	0.23:	160	0.49	150	

^aHYDRA field and aperture number of observation.

^bSources names as noted in Table 2

^cEquivalent widths in angstroms and the full-width half-maximum velocity (FWHM) in km s⁻¹ of the emission line as determined from gaussian fits. The fit parameters are greater than 5 σ unless otherwise noted. Values followed by a ":" are between 3 σ and 5 σ and values followed by a "U" are upper limits. The values for FWHM have not been deconvolved by the instrumental response.

^dThe [O II] line at 6363 Å is also observed in emission but is much weaker. In most of these objects we observe emission from [SII] at 6731 Å.

^eThe profile shape of H α as defined by Reipurth, Pedrosa, & Lago (1996): symmetric (Type I), double-peaked with the secondary peak greater than half the strength of the primary (Type II), or double-peaked with the secondary peak less than half the strength of the primary (Type III). The Roman numeral is followed by "B" if the asymmetry is on the blue side, "R" if on the red side, or "w" if the profile has non-gaussian wings. Multiple gaussian fits were used to estimate the equivalent width for Type II or III profiles. Equivalent widths for profiles with wings are lower limits. Velocity widths for Type II or III profiles are not well-defined.

^fPa 19 at 8413Å was also detected in the spectrum of WL 18 with W λ =1.9: Å and Δv =180: km s⁻¹.

^gThe Ca II emission lines display double-peaked Type IIIB profiles similar to H α .

This is Table 3 of our HYDRA paper

TABLE 4
ASSOCIATION MEMBERS

F	Ap.	Name	A_v (mag)	M(I) (mag)	LOG(T_{eff}) (K)	LOG(L/L $_{\odot}$)	M_* ^a (M_{\odot})	LOG(Age) ^a (Myr)	Notes ^b
2	15		2.6	6.26	3.512	-0.76	0.19	6.09	li,ext
2	14		2.1	8.03	3.525	-1.50	0.27	7.28	ext
2	10		0.8	8.13	3.477	-1.38	0.14	6.57	ha
1	7	SR 22	0.0	7.00	3.488	-0.98	0.15	6.18	ha,x
3	15	WLY2-3	4.9	6.04	3.544	-0.74	0.31	6.33	ha,x,ext
2	32		2.6	6.79	3.512	-0.98	0.20	6.32	x,li,ext
1	22	VSS 23	5.1	3.43	3.630	0.25	0.53	5.59	x,ext
2	25	WLY2-11	2.3	7.25	3.477	-1.03	0.14	6.17	ha,ext
1	29	SR 4	0.5	5.15	3.650	-0.43	0.91	7.01	ha,x,li
1	38	GSS 20	6.0	3.54	3.630	0.21	0.54	5.64	x,ext
3	14		1.0	7.36	3.488	-1.12	0.16	6.33	li
2	1	Chini 8	0.0	7.12	3.462	-0.93	0.12	5.57	ha,x,li
4	28		5.3	5.93	3.525	-0.66	0.22	6.06	x,ext
1	13	VSSG 19	3.4	5.05	3.544	-0.35	0.27	5.83	x,ext
2	19		2.1	6.63	3.488	-0.83	0.15	6.01	ha,li,ext
1	5	GSS 28	2.8	4.28	3.650	-0.08	0.79	6.31	ha,x,li,ext
4	39		1.9	6.06	3.512	-0.68	0.18	6.01	li,ext
2	11		0.1	7.39	3.482	-1.11	0.15	6.30	x,li
1	25	WSB 28	2.9	5.48	3.544	-0.52	0.29	6.02	ha,x,ext
4	16	GY 5	2.8	8.27	3.462	-1.39	0.11	6.47	ha,x,ext
4	41	GY 3	0.0	9.74	3.398	-1.33	<0.04	<5.0	ha,x
1	30	GSS 31	6.0	2.26	3.752	0.82	2.10	6.50	x,ext
1	28	DoAr 25	2.9	3.97	3.638	0.03	0.64	5.97	ha,x,li,ext
2	27	EL 24	7.5	3.57	3.630	0.19	0.54	5.66	ha,x,ext
4	18		2.2	8.64	3.488	-1.64	0.16	7.00	ext
4	25		1.3	9.12	3.462	-1.73	0.09	6.74	x
4	66	GY 37	3.4	9.95	3.477	-2.11	0.10	7.31	ha,x,ext
4	27	GY 59	3.491	x
2	36	WSB 34	0.8	7.80	3.488	-1.30	0.16	6.55	ha
1	2	Source 1	13	-1.15	4.278	3.20	5.00	7.60	x,ext
4	4		1.9	8.51	3.477	-1.53	0.14	6.74	ha,x,ext
2	29	WSB 37	0.8	7.00	3.477	-0.93	0.14	6.04	ha,x,li
1	21		4.3	4.83	3.591	-0.29	0.48	6.08	ext
3	22		0.4	7.74	3.488	-1.28	0.16	6.52	li
1	20	GY 112	2.4	5.92	3.525	-0.65	0.22	6.05	x,ext
4	13		4.6	6.87	3.525	-1.03	0.24	6.52	li,ext
1	36	WSB 38	7.7	1.87	3.765	0.98	2.20	6.45	ha,x,li,ext
4	30		2.8	7.62	3.488	-1.23	0.16	6.46	x,li,ext
1	32	WSB 40	5.6	3.68	3.630	0.15	0.55	5.71	ha,ext
4	53	WL 18	10.4 ^c	6.89	3.612	-0.66 ^c	0.78	7.10	ha,x,ext
2	38		1.7	7.89	3.488	-1.34	0.16	6.60	ext
4	46		8.8	5.16	3.602	-0.42	0.61	6.45	ha,ext
1	37	SR 24s	5.5	3.68	3.705	0.21	1.40	6.64	ha,x,ext
4	63		2.6	7.89	3.488	-1.33	0.16	6.59	ext
4	65	GY 204	0.5	9.25	3.462	-1.78	0.09	6.77	ha,x
4	37		6.7	6.27	3.535	-0.82	0.27	6.34	ext
3	44	WSB 45	0.0	7.43	3.488	-1.15	0.16	6.37	li,x
1	9	WSB 46	0.6	6.01	3.544	-0.73	0.31	6.31	x
3	17		8.6	4.00	3.705	0.08	1.30	6.81	ext
4	10		4.4	6.97	3.512	-1.04	0.20	6.40	ha,ext
1	6	WSB 48	0.0	7.35	3.491	-1.18	0.16	6.42	ha
...	...	SR 12	2.4	3.76	3.580	0.15	0.31	4.99	x,ext
3	6	WSB 49	0.3	7.24	3.493	-1.10	0.16	6.34	ha,x,li
4	45	GY 264	0.0	9.84	3.398	-1.37	<0.04	<5.0	ha,x
3	7		0.0	8.44	3.482	-1.53	0.15	6.80	x
2	20		1.1	7.75	3.544	-1.43	0.36	7.46	x
4	22	GY 284	4.8	7.45	3.519	-1.25	0.24	6.80	x,ext
2	6	WSB 50	1.9	7.04	3.488	-1.00	0.15	6.20	x,li,ext
4	54		3.0	6.05	3.535	-0.73	0.26	6.22	li,ext
2	35	WSB 51	4.3	3.85	3.621	0.08	0.51	5.74	ha,x,li,ext
4	24	WLY2-49	9.6	3.88	3.630	0.07	0.57	5.82	ha,x,ext
1	31	WSB 53	3.7	3.94	3.630	0.04	0.58	5.87	ha,ext
3	5	WSB 52	7.1	3.90	3.638	0.06	0.63	5.92	ha,x,li,ext

TABLE 4—*Continued*

F	Ap.	Name	A_v (mag)	M(I) (mag)	LOG(T_{eff}) (K)	LOG(L/L $_{\odot}$)	M_* ^a (M $_{\odot}$)	LOG(Age) ^a (Myr)	Notes ^b
1	26	SR 9	0.0	5.38	3.638	-0.53	0.85	7.10	ha,x,li
2	34		4.1	5.04	3.544	-0.34	0.27	5.82	x,ext
4	64	GY 326	3.544	x
3	21		0.4	7.99	3.488	-1.37	0.16	6.64	li
1	14	VSSG 14	6.7	2.24	3.895	0.94	1.70	7.15	x,ext
1	10	ROX 31	5.0	3.79	3.597	0.13	0.38	5.53	x,ext
1	24	SR 10	0.1	5.99	3.544	-0.73	0.31	6.31	ha,x
3	34	WSB 58	0.9	7.00	3.482	-0.95	0.14	6.11	x
3	31		0.9	7.11	3.477	-0.97	0.14	6.09	ha,x,li
2	3		3.0	6.21	3.525	-0.77	0.23	6.18	li,ext
2	21		3.5	6.27	3.491	-0.75	0.15	5.77	ext
3	11	ROX 32	3.5	5.69	3.525	-0.56	0.21	5.94	x,li,ext
3	20	WSB 60	2.0	7.38	3.488	-1.13	0.16	6.34	ha,ext
3	12		1.9	6.53	3.525	-0.90	0.24	6.34	ext
4	3		4.0	7.27	3.512	-1.17	0.21	6.59	ext
2	37		4.7	6.24	3.535	-0.81	0.27	6.32	ext
2	30		6.8	4.62	3.638	-0.22	0.76	6.44	ha,ext
2	4		4.8	5.87	3.544	-0.68	0.30	6.24	ext
3	39		0.5	8.61	3.477	-1.57	0.14	6.79	li
4	57		5.3	6.88	3.512	-1.01	0.20	6.36	ext
1	35	SR 20	5.7	2.08	3.747	0.89	2.20	6.41	ha,x,ext
2	23		1.4	7.73	3.482	-1.25	0.15	6.45	li
1	15	SR 13	0.0	5.07	3.491	-0.27	0.13	4.55	ha,x
3	43	WSB 63	3.8	5.37	3.553	-0.48	0.34	6.04	ha,li,ext
3	37		0.0	8.61	3.462	-1.52	0.10	6.57	li

^aMasses and ages derived relative to the theoretical tracks and isochrones of D'Antona & Mazzitelli (1997,1998).

^bAssociation membership established through the presence of H α emission (ha), x-ray emission (x), lithium absorption (li), or location above the main sequence and $A_v > 1.5$ mag (ext).

^cDue to strong emission lines in the R and I bands relative to the continuum, A_v and luminosity estimate is taken from Bontemps *et al.* (2001) using the (J-H) color and adjusted to a distance of 150 pc.